UNIVERSITY OF CALIFORNIA SAN DIEGO

Assessing Inflammatory Risks of Manufactured Polyacrylonitrile Nano- and Microplastics in Monocyte-Derived Systems *in vitro*

A thesis submitted in partial satisfaction of the requirements for the degree of Master of Science

in

Bioengineering

by

Dylan Matthew Snyder

Committee in Charge:

Professor Jack Bui, Chair
Professor Kolade Adebowale, Co-chair
Professor Pedro Cabrales Arevalo

2026

.

The thesis of Dylan Matthew Snyder is approved, and it is acceptable in quality and form for publication on microfilm and electronically.

University of California San Diego
2026

DEDICATION

The contents of this work are dedicated to the individuals who were pivotal in laying the foundation for its completion, including my family, my loving fiancée, Sara, my advisor, Dr. Jack Bui, and numerous members of the laboratory. Scientific direction, motivation, and emotional support were all key ingredients in my personal development and the evolution of this project.

TABLE OF CONTENTS

THESIS APPROVAL PAGE.....iii
DEDICATION.....iv
TABLE OF CONTENTS.....v
LIST OF FIGURES.....vii
LIST OF TABLES.....viii
LIST OF ABBREVIATIONS.....ix
ACKNOWLEDGMENTS.....xi
VITA.....xii
ABSTRACT OF THE THESIS.....xiii
CHAPTER 1: INTRODUCTION.....1
1.1 Global demand for inert polymers.....1
1.2 Ubiquitous pollution and mechanisms of clinical impact.....3
1.3 Localized interactions with the vertebrate immune system.....4
1.4 Generation, characterization, and mechanistic evaluation of MPs within immunity.....5
CHAPTER 2: PREPARING FRAGMENTATION AND CHARACTERIZATION MODALITIES FOR SYNTHETIC ORGANIC POLYMERS.....7
2.1 Polymer production and application.....7
2.2 Systematic generation of environmentally representative micro- and nanoplastics.....8
2.3 Results.....9
2.4 Discussion.....14
2.5 Methods.....17
2.6 Figures.....23
2.7 Tables.....31
CHAPTER 3: ESTABLISHING INDUCIBLE INFLAMMATORY RESPONSE IN VITRO.....36
3.1 Introduction.....36
3.2 Results.....38
3.3 Discussion.....40
3.4 Methods.....42
3.5 Figures.....47
3.6 Tables.....53
CHAPTER 4: ASSESSING PHYSIOLOGICAL RELEVANCE WITH MURINE BONE MARROW DERIVED MACROPHAGES.....54
4.1 Introduction.....54
4.2 Results.....55
4.3 Discussion.....57
4.4 Methods.....59
4.5 Figures.....63
4.6 Tables.....70

CHAPTER 5: EXPLORING HUMAN TRANSLATABILITY WITH PATIENT-DERIVED MONOCYTES....71
5.1 Introduction....71
5.2 Results....72
5.3 Discussion....73
5.4 Methods....74
5.5 Figures....76
5.6 Tables....77
CHAPTER 6: CONCLUSION....77
WORKS CITED....80

LIST OF FIGURES

Figure 2.1: Micro- and nanoplastic generation and characterization techniques……...23

Figure 2.2: SEM images of polyacrylonitrile……....25

Figure 2.3: Longitudinal observation of PAN size with dynamic light scattering…….27

Figure 2.4: LAL analysis of select microplastic preps……..…27

Figure 2.5: FTIR analysis of SPP and Sarchem stock polymers……...…28

Figure 2.6: MALDI-TOF spectra for 10 independent microplastic preps…….29

Figure 3.1: Culturing and dosing protocol for microplastic stimulation……...…47

Figure 3.2: Microplastic stimulation optimization in RAW 264.7 cells……48

Figure 3.3: Multi-polymer incubation with RAW 264.7 cells……...…49

Figure 3.4: Continued measurement of TNF-α secretion with MP/NP incubation…..….50

Figure 3.5: Increasing cell density to assess signaling impact and RNA-seq……...….51

Figure 3.6: RAW 264.7 differential gene expression and enrichment……...…52

Figure 4.1: Extraction, differentiation, and stimulation of bone marrow macrophages....63

Figure 4.2: Culturing of bone marrow-derived macrophages with plastic and LPS…....65

Figure 4.3: Inflammatory response to PAN and SAN, a copolymer…….66

Figure 4.4: New vendor, filtered, and unsonicated plastics with primary murine cells….67

Figure 4.5: Differential gene and enrichment analysis of primary murine cells……68

Figure 5.1: Evaluation of TNF-α in adhesion-enriched human monocytes……...……76

LIST OF TABLES

Table 2.1: List of polymer types, vendors, and physicochemical characteristics……31

Table 2.2: Select polymers for SEM imaging analysis……31

Table 2.3: Preps generated for longitudinal observation of particle dynamics in solution……..32

Table 2.4: Longitudinal analysis of diameter using dominant population……...32

Table 2.5: Evaluation of endotoxin in plastic preps…….33

Table 2.6: Evaluation of optical noise in microplastic preps for LAL test……..33

Table 2.7: Preparation of nonsterile PAN preps for analysis of sonication parameters……..…..34

Table 2.8: Prep size following parameter variation…….34

Table 2.9: DLS analysis of unsonicated polymers suspended in DI water…….35

Table 3.1: Polymer types and preps incubated with RAW 264.7 cells……...…53

Table 4.1: Polymer preps used in treatment of bone marrow-derived macrophages……..70

Table 4.2: Stimulating polyacrylonitrile microplastic used for bulk RNA sequencing……..70

Table 4.3: PAN preps chosen for sterile filtration……...71

Table 5.1: Microplastic preps used to stimulate monocyte-enriched PBMCs……77

LIST OF ABBREVIATIONS

PE	Polyethylene
PC	Polycarbonate
PVC	Polyvinyl Chloride
PS	Polystyrene
PAN	Polyacrylonitrile
PA	Polyamide
PP	Polypropylene
PMMA	Polymethyl methacrylate
PA 6/12	Polyamide 6/12
PA 6/6	Polyamide 6/6
PA 12	Polyamide 12
PA 11	Polyamide 11
PA 6(3)T	Poly(trimethyl hexamethylene terephthalamide)
SPP	Scientific Polymer Products
MP	Microplastic
NP	Nanoplastic
LPS	Lipopolysaccharide
RPMI	Roswell Park Memorial Institute Medium
DMEM	Dulbecco's Modified Eagle Medium
FBS	Fetal Bovine Serum
ELISA	Enzyme-Linked Immunosorbent Assay
FACS	Fluorescence-Assisted Cell Sorting

SEM	Scanning Electron Microscopy
MALDI	Matrix-Assisted Laser Desorption/Ionization
FTIR	Fourier Transform Infrared Spectroscopy
PBMC	Peripheral Blood Mononuclear Cell
BMDM	Bone Marrow-Derived Macrophage
TNF-α	Tumor Necrosis Factor Alpha
TGF-β	Transforming Growth Factor Beta
IL-1	Interleukin 1
IL-1α	Interleukin 1 Alpha
IL-1β	Interleukin 1 Beta
IL-10	Interleukin 10
IL-4	Interleukin 4
PAMPs	Pathogen-associated molecular pathways
DAMPs	Damage-associated molecular pathways
HRP	Horseradish peroxidase
TOF	Time of flight

ACKNOWLEDGMENTS

First and foremost, to my fiancée, Sara. The late nights, long days, lack of sleep, and preoccupation with life's responsibilities were difficult, but your unconditional support and love allowed me to pursue my goals and contribute to the scientific community.

I would like to thank the members of my project group. Without their expertise and assistance with experimental execution, this project could not reach its full potential.

To my advisor, Jack Bui. Your initial vision and consistent support with materials, experimental design, and troubleshooting allowed me extensive exploratory freedom.

To my family and friends. Years of persistent support and encouragement instilled my love for science and desire to offer a meaningful contribution to society. My drive to learn burns ever stronger.

I also acknowledge the use of facilities and instrumentation supported by the NSF through the UC San Diego Materials Research Science and Engineering Center (UCSD MRSEC), grant # DMR-2011924.

To the San Diego Blood Bank: a thank-you for supplying the patient-derived buffy coats for PBMC isolation.

VITA

2019	Bachelor of Science, Fordham University
2023-2024	Downstream Biologics Manufacturing, Eli Lilly & Company
2024-2025	Teaching Assistant, University of California San Diego
2024-2026	Graduate Researcher, University of California San Diego
2024-2026	Master of Science, University of California San Diego

FIELDS OF STUDY

Major Field: Immunology

Studies in Materials Science and Molecular Biology
Professor Jack Bui, MD, Ph.D

ABSTRACT OF THE THESIS

Assessing Inflammatory Risk of Manufactured Polyacrylonitrile Nano- and Microplastics in Monocyte-Derived Systems *in vitro*

by

Dylan Matthew Snyder

Master of Science in Bioengineering

University of California San Diego, 2026

Professor Jack Bui, Chair
Professor Kolade Adebowale, Co-Chair

Plastics are highly inert and environmentally persistent petroleum derivatives employed in commercial, industrial, and residential applications. Disintegration via mechanical and chemical means generates plastic fragments of micro (≤ 1 mm) or nanoscopic (≤ 1 μm) sizes. Such particles are highly heterogeneous in size, morphology, structural chemistry, and surface topography. With a vast and often indiscernible environmental burden, the biochemical and biophysical influences of plastics on mammalian physiology are of concern, especially regarding chronic inflammation. Utilizing three monocyte-derived model systems,

a mouse cell line, bone marrow-derived macrophages (BMDMs), and patient-derived, monocyte-enriched PBMCs, morphologically heterogeneous microplastics, such as polystyrene (PS) and polyacrylonitrile (PAN), at low, medium, and high dosages were imaged for topographical variety via scanning electron microscopy (SEM), size characterized by dynamic light scattering (DLS), analyzed for chemical composition by MALDI-TOF and FTIR, and screened in a TNF-α ELISA. The primary thrusts are to observe hallmark inflammatory responses to microplastic exposure, profile the physicochemical structure of polymers, and reproducibly and sterilely generate and characterize microplastics from larger fragments through sonication, microwaving, and mechanical degradation. All three cell types responded positively to PAN at sizes <1 μm and at high concentrations, with the dual upregulation of TNF-α and M2-like transcriptional programs in murine cells. Two PAN vendors differed in diameter, average molecular weight, sonication receptivity, fibrousness, porosity, and FTIR-derived chemical composition, with time-dependent aggregation tendencies. These data suggest that a microplastic derived from PAN can have biological effects on macrophages, promoting a tissue remodeling signature with preserved, antithetical mechanisms along the TNF-α axis. Future directions will include performing a mechanistic evaluation, incubating size-enriched PAN subpopulations, and screening for unknown soluble contaminants with inflammatory potential.

CHAPTER 1: INTRODUCTION

1.1 Global demand for inert polymers

Environmental contamination with anthropogenic polymers remains a complex and multifaceted phenomenon. Industrialization, population growth, commercial demand, and technological innovation have driven rapid advances in effective systems and materials for use in industries such as healthcare, construction, civil infrastructure, aerospace, and defense. Often,

these applications impose stringent requirements for chemical inertness, thermal resistance, structural rigidity, and tensile strength. Chief among those are synthetic polymer resins, commonly known as plastics. These compounds are carbon-based petroleum derivatives boasting unique chemical properties well-suited for diverse use cases. Examples include polyethylene, polycarbonate, polyvinyl chloride, polystyrene, and polyacrylonitrile. Global commercial production of these compounds began in the 1950s and quadrupled in annual output at the onset of the twentieth century.

As synthetic hydrocarbon compounds, they boast a unique set of chemical and material properties including inertness, thermal resistance, malleability, and structural rigidity. In short, case-driven synthesis can generate a tuned spectrum of materials. Production begins with crude oil, where derivatives are distilled from the parent solution, polymerized with additives, and supplied with additional inter- and intramolecular structural components or plasticizers [1]. Therefore, plastics are conglomerations with unique formulae whose properties are derived from their molecular components.

As global demand drove the amplification of synthetic polymer production, interest in biological and environmental persistence followed. Litter, single-use disposables, and limited recycling efforts, combined with physicochemical robustness, imposed an ever-growing burden of non-reactive, non-biodegradable waste, unique in size, shape, chemical structure, and surface morphology. Macroplastics are those ≥ 20 mm; particles ≤ 20 mm and ≥ 5 mm are mesoplastics. Any particulates ≤ 5 mm are microplastics, with anything ≤ 1 μm a nanoplastic [2]. Creation and distribution of these particles include distinct processes, with their generation expected to reach millions of tons [3] Primary microplastics are manufactured to the desired size, while secondary

microplastics are formed by chemical or physical disintegration. Forces including wind, hydrodynamic pressure, human-derived processes, temperature, and UV radiation supply the required energy to weaken and fragment polymers over time.

As stochastic, time-dependent processes, particle size, surface morphology, transient chemical interactions, additive shedding, and distribution in the biosphere shift with continued exposure to physical and chemical forces. Without natural processes to efficiently disintegrate plastics into their molecular components, marine, terrestrial, and atmospheric ecosystems carry their burden [2], [3].

1.2 Ubiquitous pollution and mechanisms of clinical impact

Due to their global ubiquity, the bioexposure, bioaccumulation, biomagnification, and biodistribution of micro- and nanoplastics have drawn renewed attention. Plastics have been detected in marine organisms, up the food chain to humans, with routes of exposure including inhalation, ingestion, and placental transfer. Specifically, microplastics were observed in human whole blood, livers, lungs, brains, testicles, breasts, and intestines. Goswami et al. have noted the relative concentrations of PP, PE, and PS in foods such as tuna at 1.28 microplastics per gram, energy drinks at 14 ± 5.79 microplastics per drink, chicken at 4.0 - 18.7 microplastics per kilogram, and table salt at 38.42 ± 24.62 microplastics per kilogram [4]. Characterization and quantification by Leonard et al., utilizing micro Fourier Transform Infrared Spectroscopy (μFTIR) in whole blood, identified average levels of 24 unique microplastics per liter of blood as 2467 ± 4174 in 40% of the volunteer pool [5]. Another study by Jenner et al. utilized the same methodology to characterize contamination in lung tissue. In industries such as fashion, where 60% of the fibers are synthetic, suspended secondary fibers pose an apparent pulmonary risk. Expectantly, they observed 39 different polymer types with 1.42 ± 1.50 microplastics per gram of

lung tissue, with polypropylene (PP) and polyester (PET) the most prevalent [2], [6]. These examples illustrate the substantial transfer of particulate contaminants *in vivo* among the study populations.

The synthetic and ubiquitous nature of these compounds establishes a unique lens for assessing clinical impact. The presence of particulates in the mammalian gastrointestinal system, lungs, skin, genitals, and liver warrants an investigation into local interactions with the tissue microenvironment. The literature offers propositions regarding size, shape, topography, concentration, chemical structure, and surface charge as drivers of toxicity, although distinct mechanisms of action remain unclear [6]. Additional concerns include adsorption-mediated vectoring of other known toxins. Environmental contaminants, such as heavy metals, viral proteins, and bacteria, may attach to plastics and transport into biological systems [4]. Work by Lee et al. demonstrated *in vivo* lung inflammation in mice in response to PE particles sized 10-50 μm [7]. In a separate study, Li et al. longitudinally dosed mice with polycarbonate and environmental pollutants through their feed to assess toxicity and contaminant vectoring. In treatment groups, they observed increases in reactive oxygen species production in the liver, alongside gut dysbiosis and aberrant lipid metabolism [8]. Jin et al. assessed the localization of submicron PS particles in mouse testes and reduced sperm quality [9]. Finally, Moosavi et al. noted increased bacterial response and ROS production in RAW cells [10]].

1.3 Localized interactions with the vertebrate immune system

Multiorgan localization and biochemical disruption are recurring themes across numerous studies. Consequently, interactions between particle populations and the vertebrate immune system are expected. Populations of innate immune cells, such as macrophages, and adaptive cells, such as lymphocytes, play integral roles in mediating host defense, contaminant response,

tissue remodeling, and inflammation. Discrete molecular pathways drive these phenotypes, yet these cells possess immense plasticity in response to immunogenic and immunosuppressive stimuli. As of 2025, 3,000 papers were published discussing the environmental burden of micro- and nanoplastics. In a few immunological studies, the effects of plastic exposure include a multi-organ pro-inflammatory cytokine response of TNF-α and TGF-β, mitochondrial weakening, lysosomal activation, and pro-oncogenic phenotypes [11]. Specifically, Jin et al. observed an uptick in IL-1-related cytokines, including IL-1α and IL-1β, in zebrafish. Whether through toxicity or immunogenicity, microplastics seem to both prime and kill cells of the innate immune system, as mediated by receptors, endocytosis, and reactive oxygen species [12].

Despite certain advances in understanding cell-level dynamics, the field struggles to elucidate the individual physiological relevance of particle shape, type, and crystallinity (i.e., its physicochemical properties), as well as surface morphology, transient charges, adsorptive capacity, and concentration to immune cells *in vitro* and *in vivo* [11]. In short, the breadth of results in the literature demands a standardized approach to variable reduction and an expanded investigation of additional polymers to elucidate potential mechanisms of action.

1.4 Generation, characterization, and mechanistic evaluation of MPs within immunity

This study has three independent, yet interrelated thrusts. One is to reproducibly generate chemically distinct micro- and nanoplastics from stock supplies, utilizing mechanical and electromagnetic disintegration. Second is characterizing said particles for purity, size, surface topography, and general morphology utilizing scanning electron microscopy (SEM), dynamic light scattering (DLS), matrix-assisted laser desorption/ionization time of flight (MALDI-TOF), and Fourier transform infrared spectroscopy (FTIR). Third is observing immunoresponsiveness through protein quantification assays and RNA sequencing in three distinct *in vitro* tissue

models: a mouse macrophage cell line (RAW 264.7), bone marrow-derived macrophages (BMDMs), and patient-derived, monocyte-enriched, peripheral blood mononuclear cells (PBMCs). We believe this is a powerful, multi-system analysis with physiological translatability to humans.

We sought a basic exploratory framework, acquiring a variety of common polymers, including polyethylene, polyester, polystyrene, polyacrylonitrile, styrene-acrylonitrile, polyvinyl chloride, polyamide, and polymethyl methacrylate, inducing fragmentation through sonication, microwaving, and mashing, and screening for hallmark inflammatory markers after incubating with mouse cell lines and both mouse and human primary cells. Indications of biologic activity prompted investigation of the physicochemical structure and a targeted evaluation of gene expression.

We speculate that highly polar functional groups, elevated concentration, and nanometer size are consistent drivers of certain pro-inflammatory pathways related to pathogen defense and xenobiotic response in macrophages, specifically mediated by toll-like receptors (TLRs) and NF-κB. In addition to insoluble plastic components, we surmise that soluble polymer-specific plasticizers and additives promote inflammation as measured via cytokine quantification assays. To achieve a diverse and environmentally representative treatment population, we hypothesize that less concentrated plastic solutions, when exposed to extended sonication and microwaving, produce particulates in the submicron range. In evaluating particulates post-fragmentation, we expect a heterogeneous mixture of shapes and topographical configurations, including fibers, spheres, and shards.

CHAPTER 2: PREPARING FRAGMENTATION AND CHARACTERIZATION MODALITIES FOR SYNTHETIC ORGANIC POLYMERS

2.1 Polymer production and application

Synthetic polymers are a ubiquitous environmental and biological concern. Despite this, demand enforces continued production. Items such as tires, food packaging, textiles, and industrial raw materials are produced, used, and discarded. Throughout this lifecycle, plastics are subject to degradative forces, including mechanical/hydrodynamic stresses, heat, and UV radiation [3]. Such a process is stochastic and highly heterogeneous in its output, as forces vary and material properties largely dictate the degree of fragmentation and the resulting topographies.

Consumer goods, packaging, and electronics drive the majority of plastic demand. Common packaging polymers include polystyrene, polyethylene, polypropylene, polyamide, polyimide, epoxy resins, polyurethane, and polyester. These compounds are valued for their strength, negligible reactivity under standard atmospheric conditions, malleability, low gas permeability, and minimal production costs. In textile applications, polyester is the primary material of construction [13]. To bridge application-based production with biological impact, previous work has addressed plastic (and subsequent degradation) generation with raw discovery rates in human whole-blood samples. Leonard et al. collected whole-blood samples from 20 healthy volunteers, of which 18 were analyzed utilizing μFTIR. Polymer types were identified and quantified as particles per liter of blood, less a procedural blank. Mean particle masses were then estimated using approximated densities and measured dimensions. A spectrum of particles was detected in 40% of the donor samples, including polypropylene, polyethylene, polyvinyl chloride, polyamide, ethylene-vinyl acetate, polyether urethane, and polystyrene. Total estimated

particle counts were 2465.85 ± 4173.51 microplastics per liter of blood. The group also noted the average particle size across the samples was larger than what is typically used in the literature and included both fibers and fragments [5]. Heterogeneity is both a strength and a weakness in designing realistic experimental protocols. Particulate populations with targeted distributions in size, concentration, and shape exposed to the same degree of fragmentation-inducing energy are not what are stochastically expected or physically observed. Yet, the field struggles to strategically isolate these variables for analysis during *in vitro* and *in vivo* treatments.

2.2 Systematic generation of environmentally representative micro- and nanoplastics

Commercially available microplastics typically come in the form of manufactured beads of pre-determined size. Although convenient and homogeneous, these microplastics do not resemble nor model the particles that accumulate in human and animal tissue. Previous research has outlined methods to generate microplastics in place of vendor-sourced materials. For example, Lee et al. generated 10-50 μm polyethylene microplastics via grinding cryogenically frozen 5 mm beads for oral introduction into mice [7]. Tolardo et al. employed laser ablation to generate polycarbonate microplastics as a model for an aquatic environment [14]. To better model microplastic heterogeneity, shape, and potential biologic activity, we sought to reproducibly generate micro- and nanoplastics across a variety of polymer types—PAN, PSU, PS, PC, PA 6/12, PA 6/6, PA 12, PA 11, PA 6(3)T, PVC, PMMA, and SAN—using three distinct modalities to mimic environmental conditions: bath sonication, microwaving, and physical mashing with a blunt object. To visualize the breadth of the particle population, the hydrodynamic radius was measured by DLS, size and surface topography by SEM, polymer identity by FTIR, and chain length by MALDI-TOF. The immense diversity of our polymer set and streamlined generation protocol is a novel, environmentally and physiologically relevant

approach in treatment population creation that does not rely on a limited selection of manufactured beads of pre-determined size.

Additionally, we sought to examine particles that exhibited some solubility in aqueous solution, as these would likely have the greatest potential to exert biological effects. Moreover, the water-soluble fraction of plastic polymers is likely equally important in assessing exposure profiles during everyday activities. Water-soluble fractions of polymers have been described by Qin et al., who demonstrated the degradative capacity of various solvents, including deionized water, to shed irregularly shaped microplastics from bulk polycarbonate films over 250 days [15]. Finally, in generating material for *in vitro* treatment, we sought to observe how time, temperature, the degree of ionizing radiation, and energy density affect material degradation. In doing so, we provide a diverse and comprehensive formulation and characterization architecture with outstanding potential to elicit one or more variables acting as inflammatory stimuli in innate immune cells.

2.3 Results

To examine the interface of the soluble and insoluble fractions of plastics, we added 15 to 40 mg of 14 unique plastic polymers obtained from commercial sources to 1 mL of deionized water. The mixtures were subjected to sonication, mechanical crushing, and/or microwave to create preparations (preps) that had a visible fraction of particulates. In total, 117 preps were generated utilizing 14 different polymers, specifically PAN, PS, PA 6/12, PA 6/6, PA 12, PC, PSU, PVC, PMMA, and SAN, which were later used in cell culture treatment (Table 3.1, Table 4.1). A significant majority of the compounds, including the polyamides, polysulfone, and polycarbonate, failed to produce any resolvable (visible by DLS) particulates following the standard sonication protocol. Physically, these compounds came in pellet form and were rigid in

structure. Other powdered polymers, like PAN, PS, and PMMA, were easily fragmented. At 30 minutes of sonication, PAN showed a relative size of 520.7 nm versus 1452.17 nm in the unsonicated control, a 3x reduction in the average diameter of the population. In PMMA, the unsonicated prep was 771.55 nm, with 30 minutes of sonication producing 555.05 nm (Table 3.1 and Table 2.9). Regarding its biological properties (see results in Chapter 3 below), one specific polymer, polyacrylonitrile (PAN), was selected for extended analysis.

2.3.1 Topographical and morphological observation of PAN particles

We used scanning electron microscopy to obtain images of PAN particles sonicated for 90 minutes. SEM settings were tuned for a 3.00 kV acceleration voltage. Low-magnification images of ethanol-dispersed PAN particles (Prep ID: 2H3) documented a heterogeneous population of PAN particles, ranging in size from 50 nm to 2 μm. Shapes included spheres, irregular spheroid configurations, and fibers. This compound displays a smoother topographical structure with distinct nanoscopic domains of either individual particles or potential aggregates (Fig. 2.2a). The same prep dispersed in DI water exhibited similar morphology, with a clearer view of a monolayer (Fig. 2.2c). A higher-magnification image details a seeming cluster of nanoparticles or roughly textured microparticles, with fibers interspersed between the clusters (Fig. 2.2c and 2.2d). DLS analysis of Prep 2H1 measured an average diameter of 294.13 nm (Table 2.2).

Sarchem PAN (Prep ID: 2H1 and BM1), a different vendor for PAN, was imaged dispersed in pure ethanol (2H1) and water (BM1). At low magnification, 2H1 displayed a porous, smooth, spherical structure with diameters around 1 μm, with larger particles 5-10 μm (Fig. 2.2e). BM1 showed microplastic-sized particles with minimal observed aggregation.

Particles were rounded, highly porous, and measured 10 to 20 μm. DLS results indicated an average size of 1,135 nm (Fig. 2.2f and 2.2g).

2.3.2 Hydrodynamic radius of PAN polymer as a function of time

To study the stability of the preps over time, we stored preps at room temperature and measured their diameters via DLS. Following 30 minutes of sonication, the preps exhibited baseline size profiles ranging from 219.1 nm to 358.1 nm. After one week of room temperature storage, average diameters roughly doubled and tripled, with the largest difference of 1166.1 nm in prep L5. The highest concentration preps, L5 and L6, increased substantially in size. After two weeks, preps decreased in size, with only L3 increasing 41.7 nm to 525.4 nm. Group divergence in size occurred after one month, with L1 and L5 increasing 165.23 nm and 111.5 nm, respectively. At 35 days, L1 decreased by 41% and L5 by 44%, while the remaining preps showed less significant changes. By day 59, preps were within 227.5 nm of their baseline. L6 on Day 59 generated inconclusive size results and was removed from the analysis (Fig. 2.3 and Table 2.4).

2.3.3 Assessment of endotoxin as potential stimulator in sterile preps

Using the conversion factor provided by GenScript, the LPS concentration of the prep with the largest endotoxin burden, when correcting against the water control, is 0.0333 ng/mL (Fig. 2.4a and Table 2.6). Since PAN remained suspended in the LAL reagents and was exposed to the 545 nm laser (the vendor-recommended wavelength for absorbance measurement), a background signal analysis at that wavelength was performed against PAN at 26.80 mg/mL and a tenfold to thousandfold dilution. A maximum average optical density of 0.74125 was observed in

the highest concentration aliquot. With the initial tenfold dilution and reagent addition, it is approximated that PAN contributed 50% to the observed absorbance. Note that for cell culture, levels should be < 0.1 to 1 EU/mL (0.01 to 0.1 ng/mL).

2.3.4 Effect of duration, concentration, and water bath characteristics on PAN microplastic size following bath sonication

Similarly concentrated preps exposed to bath sonication in 15-minute intervals in middle and corner locations within the instrument generated an average diameter in the most prominent population of 210.5 nm ± 12.30 and 642.6 nm ± 7.423, respectively. At a 30-minute interval in corner and middle locations, preps exhibited an average diameter of 496.1 nm ± 263.5 and 305.5 nm ± 127.3. To assess effects of bath volume, preps placed in the sonicator corner and middle and suspended in 500 mL of room temperature water recorded average diameters of 560.0 nm ± 118.8 and 179.1 nm ± 2.687, respectively. An unsonicated control was measured at 3536 nm (Table 2.8).

PAN destined for incubation in cell culture was sonicated across various durations and concentrations. An initial measurement of PAN sonicated at 30 mins, 1 hour, and 2 hours (at similar concentrations) showed average diameters of 520.7 nm, 525.7 nm, and 469.2 nm, respectively (Table 3.1). Another PAN prep generated at 24.28 mg/mL and 30 minutes of sonication showed an average diameter of 580.13 nm. At lower concentrations, for example, 12.76 mg/mL and 60 minutes of sonication, PAN displayed an average diameter of 385.8 nm. When the prep concentration was increased to 23.0 mg/mL, 47.0 mg/mL, and 58.0 mg/mL at the same sonication duration, diameters were 435.3 nm, 462.7 nm, and 384.9 nm, respectively (Table 3.1). We did not see any trends in sonication time and concentration in determining particle size

as measured by DLS, except for unsonicated controls (Table 2.9). Although similarly concentrated preps with similar fragmentation durations showed loosely related size profiles, demonstrating reproducibility, we cannot predict or find any correlation between sonication time and concentration with particle size.

2.3.5 Confirmation of two vendor polymer identities

When corrected against the baseline, both stock polymers of PAN sourced from SPP or Sarchem vendors showed distinct, sharp absorbance peaks at 2200 wavenumbers, a known identifier for the nitrile group. Additional peaks occurred around 3100 and 1450 wavenumbers, indicative of a C-H bond and the molecular fingerprint region, respectively. Sarchem-sourced PAN was shifted higher in absorbance across the spectra. A cosine similarity analysis between uncorrected spectra yielded a 95.72% similarity, with 99.36% within the 2200 wavenumber region (Fig. 2.5).

2.3.6 Qualitative analysis of polymer length and identity

Across the measured preps, the spectra displayed interpeak differences of approximately 53.06 g/mol, one PAN monomer. The matrix solution displayed strong M/Z ratios between 400 and 800 kDa, with a sharp peak at 810 kDa. SPP PAN with 1.5-hour sonication showed distinct peaks arising at 289.30, 333.45, 559.91, and 612.83 kDa (Fig. 2.6b). SPP at 30 minutes of sonication showed peaks at 267.89, 311.19, and in the 400 kDa region (Fig. 2.6c). SPP PAN 30 minutes of sonication and microwaving had a denser collection of peaks below 700 kDa, specifically at 289.07, 400, and 610 kDa (Fig. 2.6d). Sarchem PAN after 30-minute sonication had similar density, with notable peaks at 267.0, 289.0, 325.3, and 497.7 kDa (Fig.

2.6e). Another Sarchem PAN prep with 30-minute sonication displayed peak separations between 267.93 and 311.2 kDa, with peaks occurring beyond 1,000 kDa (Fig. 2.6f). Unsonicated SPP SAN had peaks between 200 and 300 kDa (Fig. 2.6g). Sarchem PAN with 2 minutes of microwaving and 6 hours of sonication displayed peaks within the 1000 kDa range, with 600 - 900 kDa the most prominent (Fig. 2.6h). A Sarchem prep with just 6 hours of sonication displayed a similar size profile, with peaks around 615 to 800 kDa, with greater peak density around 200 kDa (Fig. 2.6i). Unsonicated SPP PAN displayed numerous high-intensity peaks, with those sitting at 268.04, 311.28, 615, and 725 kDa (Fig. 2.6j). Finally, Sarchem PAN sonicated for 30 minutes displayed peak intensity at 311.18 kDa, with other peaks around 350 and 400 kDa. Max M/Z ratios peaked around 1314 kD across all samples. SAN showed weaker intensity values in both samples across their respective spectra. Additionally, SPP PAN measured larger max M/Z ratios (Fig. 2.6).

Beginning with the first sample, there are 42, 30, 42, 46, 45, 36, 30, 39, 39, and 27 total peaks, respectively. Of those total peaks per sample, there are 17, 17, 7, 13, 9, 1, 13, and 1 peak(s) in the PAN samples separated by the molecular weight of one PAN polymer, respectively. SAN polymers, with 30 minutes of sonication, displayed 8 peaks with a spectral width of styrene (Fig. 2.6).

2.4 Discussion

We assessed 14 polymers and found that a subset of these had particles detectable by DLS analysis. Through size, chemical, and morphological analysis, we observed that micro- and nanoplastic generation was a polymer- and vendor-specific phenomenon. For the non-fragmented polymers, the combination of their native pellet form and material properties driven by strong intermolecular forces supplied the likely resistance to more powerful forms of energy.

The bath sonication at room temperature for 30 minutes to 2 hours was likely insufficient in supplying a focused energy source powerful enough to degrade these polymers, or the particles shed from the compound were below the detection limit of the Zetasizer. Despite this, it is not known why certain polymers displayed measurable fragmentation in the collected fractions compared to other polymers. Larger molecules or polymer chains (plastics with carbon backbones) that exhibit similar profiles of electrostatic interactions (Van Der Waals forces, London dispersion forces, etc.) have proportionally greater intermolecular forces. However, per Table 2.2, the average molecular weights (MW) of the polymers, PAN being one of the largest, do not match this relative susceptibility to fragmentation. It is possible that the nitrile group of PAN permitted spontaneous or sonication-induced fragmentation in water. If so, the physiologic relevance of this is clear—PAN polymers exposed to aqueous solutions should shed soluble fragments with potential biologic activity.

Therefore, we conclude that the degree of fragmentation in PAN is largely stochastic from prep to prep and with time. To assess this, we performed a longitudinal analysis of size using six independent PAN preps with similar fragmentation characteristics and manipulated sonication parameters to assess impacts on average size. Over 59 days, the ZetaSizer displayed divergence in size profiles to 3 times the baseline size, with all returning close to and above the baseline. Interestingly, even amongst preps of the same concentration, baseline diameters varied by upwards of 139 nm in L3 and L4. In the next measurements, the highest concentration preps, L5 and L6, increased substantially in size, likely from the influence of more frequent localized interactions enforcing aggregation. The measurements listed in Table 2.4 suggest an aggregation dynamic driven by hydrophobic particle interactions in aqueous solution. PAN is a largely hydrophobic compound, with the primary moiety, a polar nitrile group. These behaviors directly

impact the size of particles seen by cells. Aspects of sonication as a fragmentation modality, not just sonication time, are also important in determining size profiles. Factors, including bath volume, tube location within the bath (regions of higher energy density), and continuity of supplied energy, all impact average diameter (Table 2.8). In general, the larger average particle size in the bath corners suggests sound waves are concentrated in the center. Additionally, sonication intervals (units of 15 minutes) suggest a fluctuation in energy output. Finally, reducing the bath volume with preps centered generated the smallest-sized particles. Reduction in volume means less mass for the waves to travel through, preservation of mechanical energy, and a faster increase in bath temperature, thus supplying a larger, sustained energy supply to the polymers.

We performed SEM imaging of the plastics to assess physical characteristics, using two independent PAN vendors. SPP PAN (Prep ID: 2H3) in DI water showed distinct sizes between 0.25 and 1.0 micron. The clumping pattern indicates a multilayered aggregation of smaller particles and fibers. It is unknown if the aggregates seen are representative of those in solution; however, DLS is sensitive to aggregates when particles are clumping due to hydrophobic forces or surface characteristics. Therefore, it is likely the true size of the particles
is smaller than what DLS measures (Fig. 2.2a and 2.2b). EtOH dispersion showed a similar aggregation pattern (Fig. 2.2c and 2.2d). In both cases, the particles were topographically diverse, with smooth and pointed features. The Sarchem PAN images (Prep ID: 2H1) display particles of much larger size (3 to 8 μm), with porous topography and more rounded morphology. Interestingly, the DLS data for Sarchem PAN preps showed sizes around and over 1000 nm across numerous preps. For example, PAN sonicated for 1.5 hours measured 973.07 nm (Table 4.1). This PAN was more resistant to change in size with similar fragmentation modalities to SPP. With average particle sizes over 1 micron, despite the average molecular weight of

70,000 g/mol versus 150,000 g/mol for SPP, it suggests a greater aggregation tendency (i.e., a difference in surface chemistry) or a milling process that generates larger particle sizes (Fig. 2.1). Generally, the two PAN stocks, despite bearing the same polymer chemistry, differed in size and morphology.

For chemical and degree of fragmentation analysis, we performed FTIR and MALDI-TOF. Both Sarchem and SPP PAN displayed the same distinct peak at 2243 cm^{-1}, indicative of a nitrile group. Additional peaks around 2800-3000 cm^{-1} indicate the presence of C-H bonds. Other peaks around 1200 cm^{-1} occur in a fingerprint region, which is suggestive of other unknown chemical groups. Additionally, Sarchem PAN exhibited a slightly higher absorptive capacity over SPP along the spectra (Fig. 2.5). In the MALDI-TOF analysis, the peakwise differences across numerous preps were indicative of degrees of fragmentation by one monomer. Interestingly, the polymer size-to-charge ratio, specifically the molecular weight, capped around 1,000 g/mol. When compared to the respective average molecular weights supplied by the vendor and instrument-limited detection below 100,000 g/mol, the resolvable population measured only a few monomers long, suggesting a significant nanoscopic population. Such findings bolster the theory of aggregation and a distinct dispersion of particle size.

Before incubation in culture, preps were assessed for pre-existing inflammatory molecules, like LPS, as plastics were not purchased endotoxin-free. We observed no impactful burden of endotoxin. At the highest concentration of 0.0333 ng/mL, the LPS burden measures below the threshold for low-dose BMDM activation of 50 pg/mL [16].

2.5 Methods

2.5.1 Acquisition of bulk polymer material

Plastics were sourced from multiple vendors. Polystyrene (4.8 - 5.8 μm, 1.03-1.05

g/cc; 200 mg) and polyethylene (200 - 9900 nm, 0.95-0.98 g/cc; 1 g) microspheres were purchased from Cospheric, LLC (Cospheric, LLC., Santa Barbara, CA, USA). Bulk powders and beads were purchased from Scientific Polymer Products (Ontario, NY). This included polystyrene (1,200 g/mol, 1.06 g/cc), low-density polyethylene (50,000 g/mol, 0.92 g/cc), polyacrylonitrile (150,000 g/mol, 1.184 g/cc), polycarbonate (36,000 g/mol, 1.20 g/cc), polysulfone (60,000 g/mol, 1.24 g/cc), Nylon 6 [Poly(caprolactam)] (25,000 g/mol, 1.14 g/cc), Nylon 6(3)T [Poly(trimethyl hexamethylene terephthalamide)] (1.12 g/cc), Nylon 6/6 [Poly(hexamethylene adipamide)] (1.30 g/cc), Nylon 6/10 [Poly(hexamethylene sebacamide)] (15,000 g/mol and 25,000 g/mol, 1.08 g/cc), Nylon 11 [Poly(undecanoamide)] (1.04 g/cc), Nylon 12 [Poly(lauryllactam)] (1.02 g/cc), Poly(methyl methacrylate) (15,000 g/mol, 1.20 g/cc), Poly(vinyl chloride) (130,000 g/mol, 1.40 g/cc), and styrene/acrylonitrile copolymer (185,000 g/mol, 1.07 g/cc). A secondary bulk polyacrylonitrile powder (70,000 g/mol, 1.184 g/cc) was purchased from Sarchem Labs (Farmingdale, NJ).

2.5.2 Weighing and assembly of preps

Sterile FACS tubes (Falcon; Cat #: 14-959-6, San Diego, CA, USA) were obtained, labeled, and weighed (Mettler Toledo, *AT261 DeltaRange*; Columbus, OH, USA). Procedures were performed in a laminar flow hood (Nuaire; Plymouth, MN, USA). Using a sterile, sloped edge, a portion of the choice polymer was removed from its bulk container and placed into the FACS tube. The filled tubes were then weighed (Mettler Toledo, *AT261 DeltaRange*; Columbus, OH, USA). Preps were measured between 15 and 40 mg, according to experimental need. Preps were resuspended in 1 mL of deionized, UltraPure water (Gibco; Waltham, MA, USA) and stored in the dark at room temperature before fragmentation.

2.5.3 Preparation of fragmentation modalities

Preps were fragmented using one to two modalities: bath sonication (Branson, *Branson 1800*; Brookfield, CT, USA), microwaving (Kenmore; Hoffman Estates, IL), and mechanical mashing with a sterile inoculating loop (CellTreat; Ayer, MA). For bath sonication, the basin was filled with 1L of deionized water. Preps were placed within a tubing rack and secured with a weight. Preps were sonicated for 30 minutes, 1 hour, 1.5 hours, or ≥ 2 hours. For microwaving, preps were mixed, placed on a paper towel, and microwaved for 2 minutes. For mashing, preps were placed in the sterile hood with an inoculating loop. For 1 minute, the solution was stirred and agitated with a consistent hammering motion. Preps were stored in the dark at room temperature after fragmentation.

2.5.4 Characterization of hydrodynamic radius with dynamic light scattering (DLS)

100 µL of the chosen preps were aliquoted into 1.5 mL Eppendorf tubes and analyzed within the materials science and engineering core (UCSD MRSEC; San Diego, CA, USA). 50 µL of each prep was dispensed into a cuvette (Malvern; Malvern, UK) and placed into the sample chamber of the instrument (Malvern, *Malvern Instruments Zetasizer Nano*; Malvern, UK). Acquisition settings were tuned to perform triplicate measurements, with a 60-second equilibration period and polypropylene as the reference material. The final z-average diameter, the average diameters across each normally distributed population, and the diameter of the most prominent population in a multimodal distribution were averaged and recorded.

2.5.5 Characterization of three-dimensional structure with SEM

Preps were allowed to settle and shaken gently before aliquoting. 50 uL was removed from the upper fraction of liquid and diluted 10-fold with DI water or pure EtOH to assess dispersant capability (Gibco; Waltham, MA, USA). Then, 10 uL of the diluted preps were dispensed onto glass slides and gently spread with the pipette tip. Slides were placed in the chemical fume hood and allowed to dry for ≥ 4 hours. Next, circular carbon tape (Ted Pella, Inc.; Redding, CA) was attached to the sample stages. Then, the dried sample powders were gently pressed against the carbon tape. Prepared sample stages were taken to the Nano3 core facility and coated with an iridium nanolayer. Samples were imaged using the Zeiss Sigma 500 Scanning Electron Microscope (Zeiss, USA); settings were tuned to an SE2 detector and a 3.00 kV acceleration voltage.

2.5.6 Characterization of functional group chemistry with FTIR

In preparation for FTIR analysis, stock polymers of choice were removed from their containers and placed into 1.5 mL Eppendorf tubes (Thermo Fisher Scientific; Waltham, MA, USA). Samples were taken to the materials characterization core at UCSD MRSEC (San Diego, CA, USA). Samples were handled with a weighing spoon and gently packed into the detection window. A background spectrum was collected using the LaTGS detector with ATR correction with a spectral range between 350 and 7,800 wavenumbers (Thermo Fisher Scientific, *Nicolet™ iS50 FTIR*; Thermo Fisher Scientific; San Diego, CA, USA). Then, the sample was gently packed into the detection window using a weighing spoon and compressed with the sample restraining arm. A spectrum was recorded and auto-corrected with the background. Note that the native polymer was analyzed instead of the fragmented population.

2.5.7 Characterization of the degree of fragmentation with MALDI-TOF

Stock 50 uL aliquots of select fragmented polymers were prepared. In preparation for matrix-assisted laser desorption/ionization time of flight (MALDI-TOF), 1 μL of the prep was mixed on a sequencing chip with 1 μL supersaturated solution of α-Cyano-4-hydroxycinnamic acid (Bruker, *MALDI-TOF BioTyper*; Billerica, MA, USA). An HCCA negative control was also dispensed. Sample locations were dried with a heat gun and inserted into the sampling chamber. Measurement parameters were set for the negative ion laser and a mass range of 240 to 51200 Daltons with a linear detector gain of 2557V. Generated spectra were qualitatively compared utilizing a large language model.

2.5.8 Longitudinal observation of particle size in aqueous solution

To observe particle dynamics in aqueous solution post-fragmentation, six PAN (Scientific Polymer Products; Ontario, NY) solutions were prepared at concentrations between 24.12 mg/mL and 38.57 mg/mL in deionized water (Gibco; Waltham, MA, USA) and bath sonicated for 30 minutes using the above protocol in Chapter 2, section 2.5.3. Samples were stored in the dark at room temperature. Baseline size at t_0 was analyzed via DLS (Malvern, *Malvern Instruments Zetasizer Nano*; Malvern, UK) using the settings detailed in Chapter 2, section 2.5.4. Subsequent measurements were performed at 7, 14, 31, 35, 43, and 59 days. Additional preps spanning polymer type were diluted by half and measured at one time point post-generation.

2.5.9 Analysis of lipopolysaccharide (LPS) using limulus amoebocyte lysate (LAL) in MP preps

Assessment of LPS contamination was performed on six random preps with potential inflammatory response. Preps were brought into the hood, diluted two-fold with deionized UltraPure water (Gibco; Waltham, MA) to limit chunking, aliquoted into 250 uL volumes, and vortexed to disperse and agitate solutes. Test performance commenced in accordance with the vendor protocol (Genscript, *ToxinSensor™ Chromogenic LAL Endotoxin Assay Kit;* Nanjing, China). One prep was aliquoted and diluted 1/10, 1/100, and 1/1,000, then measured at 545 nm in a 96-well plate in pure, deionized water (Gibco; Waltham, MA, USA) to assess optical noise (Molecular Devices, *SpectraMax M2* Plate Reader; San Jose, CA). Prep conditions are listed in Table 2.7.

2.5.10 Analysis of sonication parameters on fragmentation stochasticity using nonsterile preps

Polyacrylonitrile (Scientific Polymer Products, Ontario, NY) was removed from the stock bottle in the laminar flow hood and placed in a 50 mL conical tube (Gibco; Waltham, MA, USA). Due to the removal method, fewer fine particles were isolated. The bulk allotment was ground in a mortar and pestle to produce fine particulates with a texture similar to that of the sterile preps generated per Chapter 2, section 2.5.3. Then, ground PAN was weighed into preps in accordance with applicable testing parameters listed in Table 2.7. Size was determined by DLS, per Chapter 2, section 2.5.4.

2.6 Figures

Figure 2.1. Overview of micro- and nanoplastic generation and characterization techniques. (a) Stepwise production framework for micro- and nanoplastics from bulk stocks. Preps were weighed out to 20-40 mg and resuspended in 1 mL of Ultrapure, deionized water. Polymers were subjected to 30 minutes to ≥ 2 hours of sonication, 2 minutes of microwaving, and/or 1 minute of mashing. Fragmented polymers were analyzed for size via DLS, identity and chemical surface characteristics via FTIR, morphology via SEM, and degree of fragmentation with MALDI-TOF. **(b)** For SEM, 10 µL of preps, diluted tenfold, were aliquoted onto plain glass slides or those affixed with carbon tape. Preps were allowed to dry for ≥ 4 hours and qualitatively assessed for high-resolution particle morphology. **(c)** MALDI-TOF analysis was performed by dispensing 1 µL of HCCA and 1 µL of polymer onto a sequencing chip, alongside an HCCA control. Samples were dried and sequenced with a negative ion UV laser. **(d)** For FTIR, the bulk solid polymer was handled with a weighing spoon and packed into the detection window. Polymers were analyzed for molecular identity with a LaTGS detector with ATR correction, with an infrared spectral range between 350 and 7,800 wavenumbers. **(e)** Size analysis of polymers, before and after fragmentation, via DLS, involved dispensing 50 µL into a plastic cuvette, performing a 60-second sample equilibration, and capturing Z-average and population-based hydrodynamic radii.

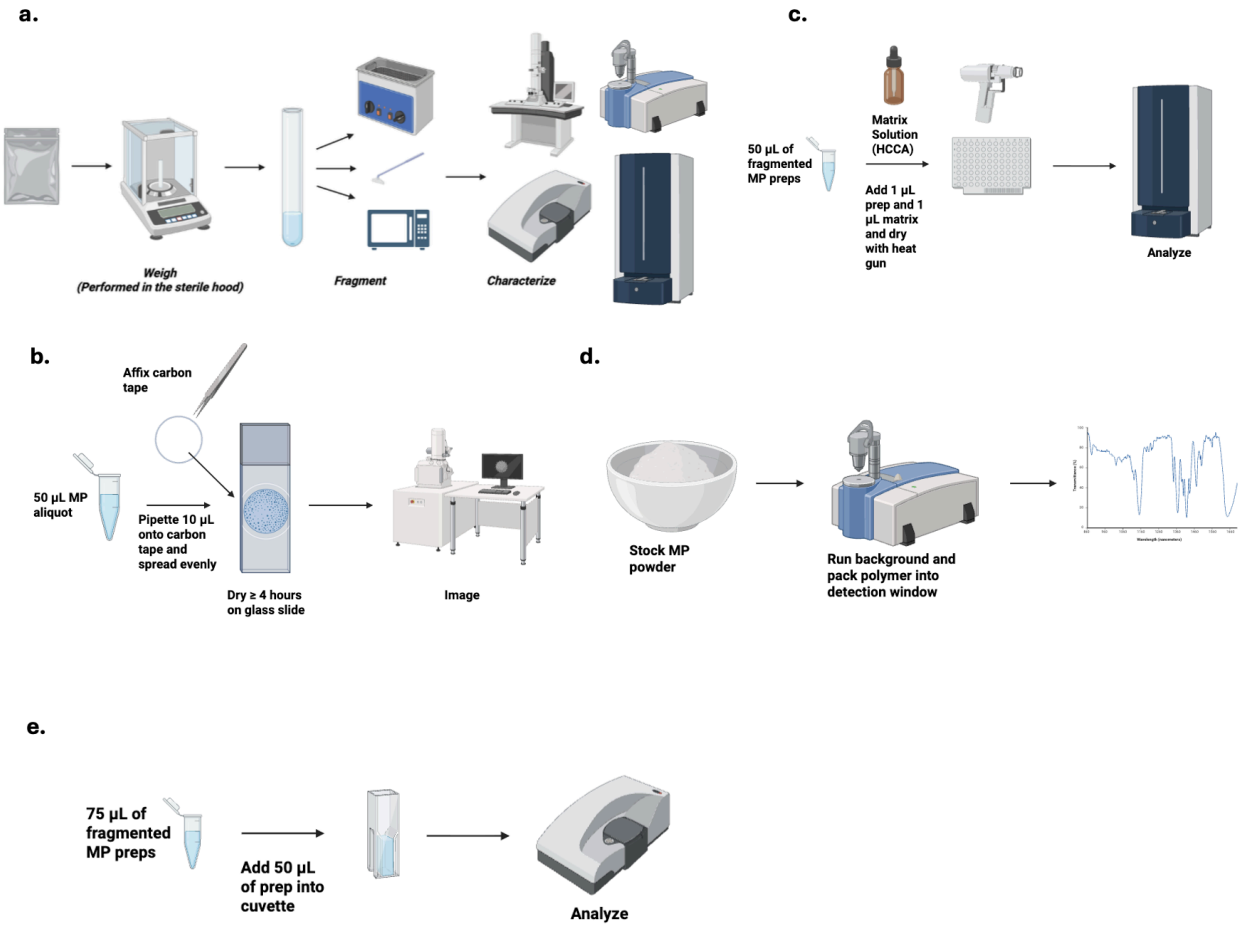
a.
Weigh
(Performed in the sterile hood)
Fragment
Characterize
c.
50 µL of fragmented MP preps
Matrix Solution (HCCA)
Add 1 µL prep and 1 µL matrix and dry with heat gun
Analyze
b.
Affix carbon tape
50 µL MP aliquot
Pipette 10 µL onto carbon tape and spread evenly
Dry ≥ 4 hours on glass slide
Image
d.
Stock MP powder
Run background and pack polymer into detection window
e.
75 µL of fragmented MP preps
Add 50 µL of prep into cuvette
Analyze

Figure 2.2. SEM images of Scientific Polymer Products and Sarchem Labs PAN. Sonicated preps of Sarchem and SPP PAN were resuspended in deionized water or pure EtOH and dried on glass slides. Carbon tape was affixed to sample stages and pressed into the powders. Samples were imaged at an acceleration voltage of 3.00 kV using the Zeiss Scanning Electron Microscope.

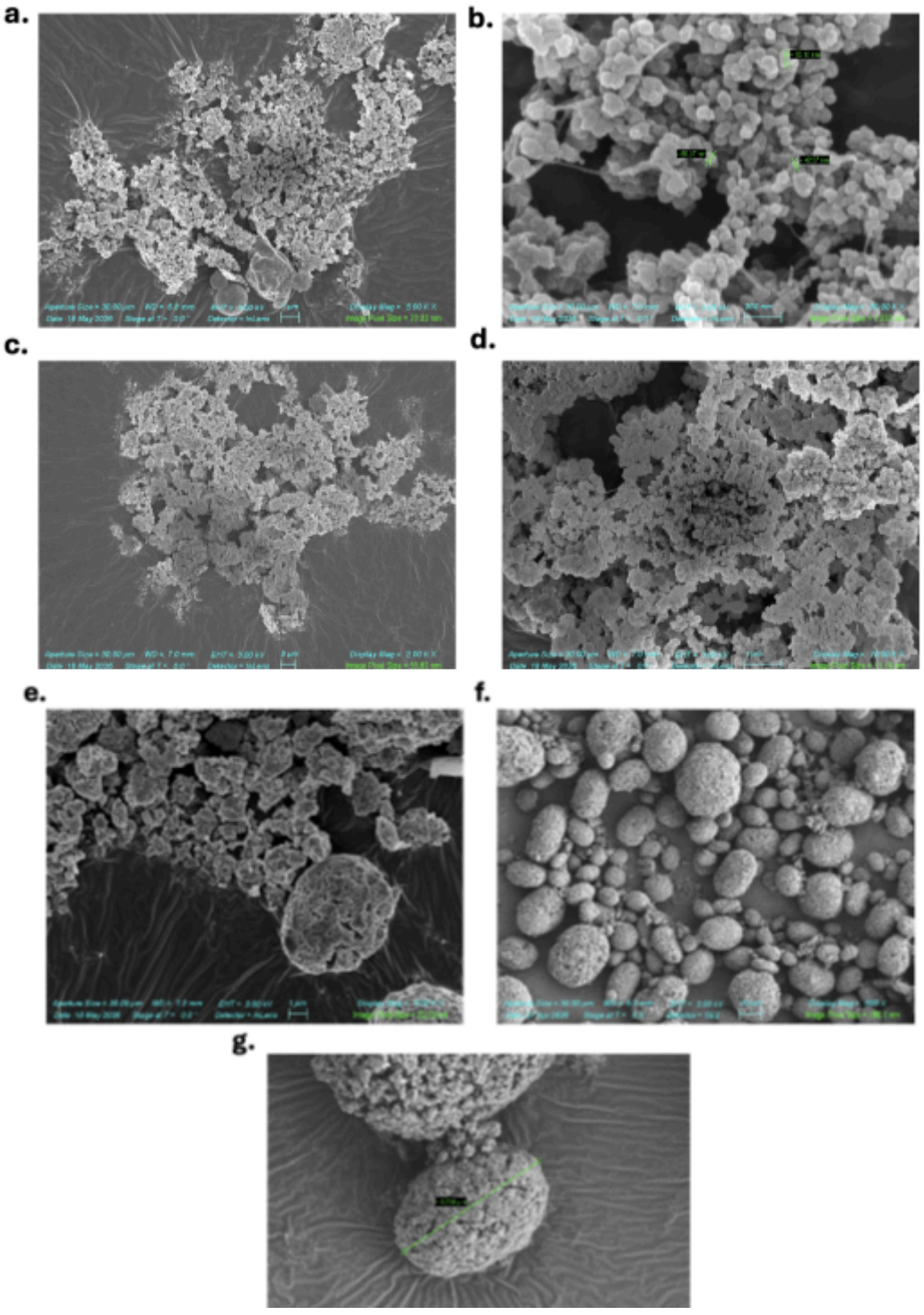
a.
b.
c.
d.
e.
f.
g.

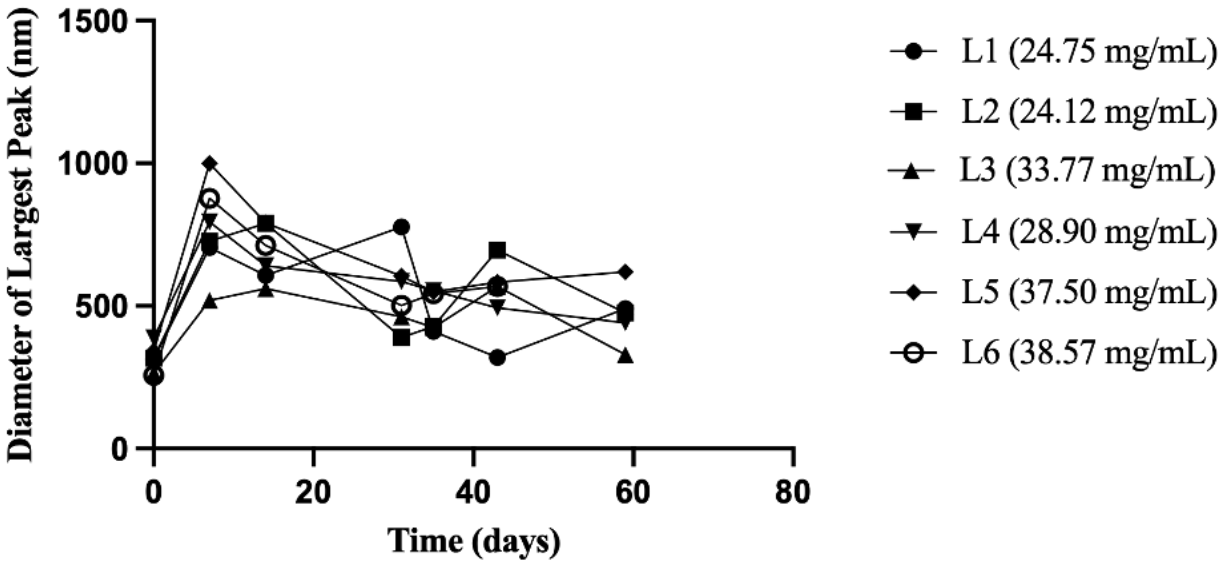

Figure 2.3. Longitudinal observation of PAN size at room temperature via DLS. Stock SPP PAN was sonicated for 30 minutes at varying concentrations listed in Table 2.4. Baseline diameters were recorded with time points up to 2 months post-preparation. Preps were stored at room temperature in the dark.

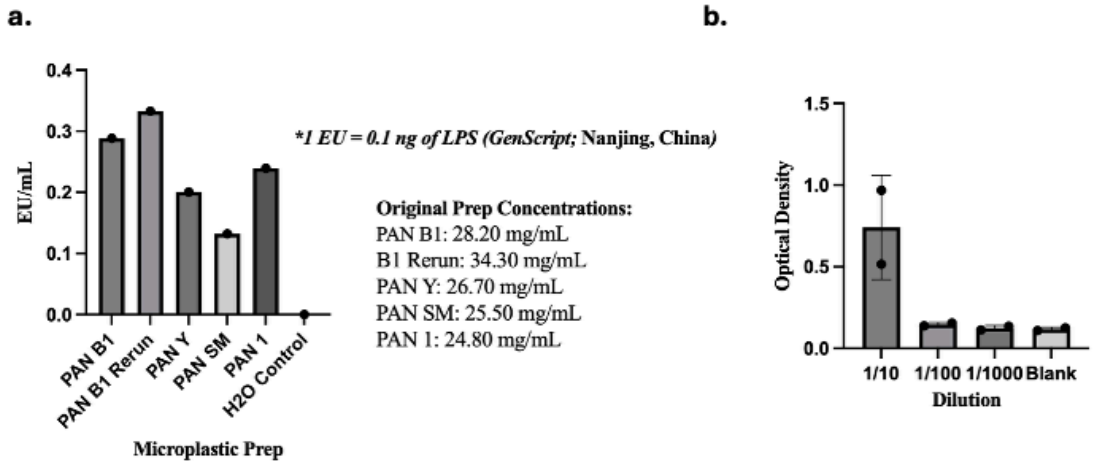

Figure 2.4. LAL analysis of select microplastic preps. (a) An LAL analysis was performed on five preps in duplicate to assess LPS contamination. Values were estimated as means only; no standard deviations were calculated. **(b)** Stock PAN solution was prepared at 26.80 mg/mL and sonicated for 1 hour. Absorbance was measured at 545 nm to assess noise and subtracted from raw values to obtain concentrations listed in (a).

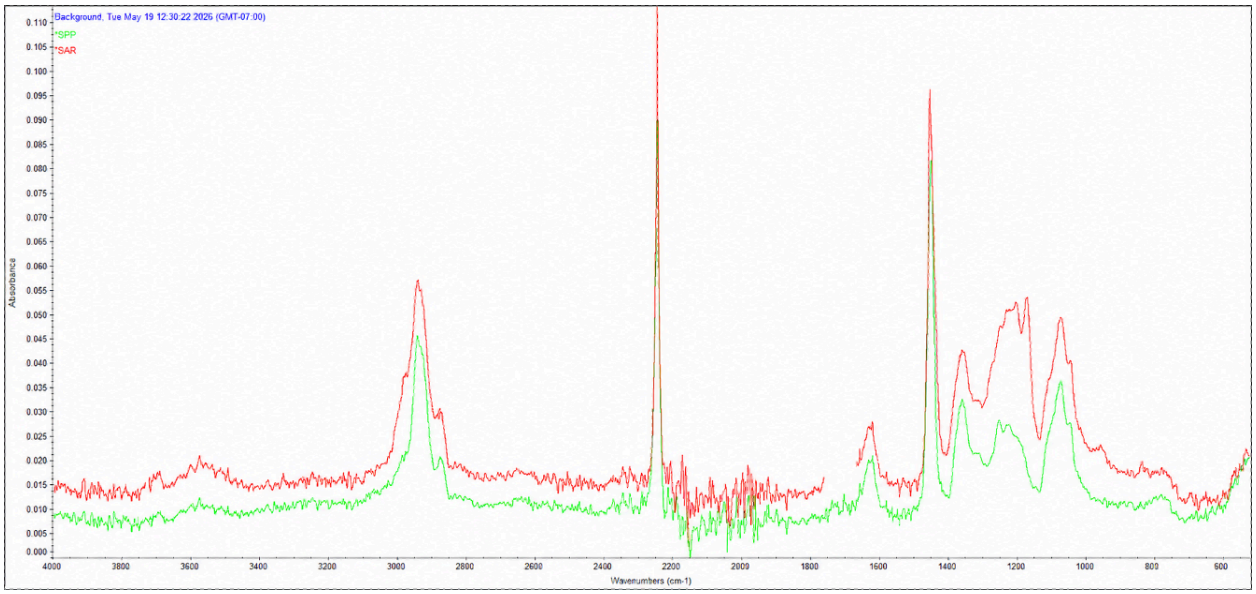

Figure 2.5. FTIR analysis of SPP and Sarchem stock polymers. Baseline-corrected spectra were generated for solid stock PAN polymers, with prominent peaks such as the nitrile signal (around 2243 cm^{-1}) assessed to confirm polymer identity.

Figure 2.6. MALDI-TOF spectra for 10 independent PAN and SAN preps with a mass range of 240 to 51200 Daltons with a linear detector gain of 2557V. (a) Matrix solution spectra. **(b)** SPP PAN (1.5-hour sonication; 25.5 mg/mL). **(c)** SPP SAN (30 minutes sonication; 21.5 mg/mL). **(d)** SPP PAN (2 minutes microwave + 30 minutes sonication; 31.3 mg/mL). **(e)** Sarchem PAN (30 minutes sonication; 34.7 mg/mL). **(f)** Sarchem PAN (30 minutes sonication; 21.2 mg/mL). **(g)** SPP SAN (Unsonicated; 29.1 mg/mL). **(h)** Sarchem PAN (2 minutes microwave + 6 hours of sonication; 30.6 mg/mL). **(i)** Sarchem PAN (6 hour sonication; 34.4 mg/mL). **(j)** SPP PAN (Unsonicated; 28.2 mg/mL). **(k)** Sarchem PAN (30 minutes sonication; 29.3 mg/mL).

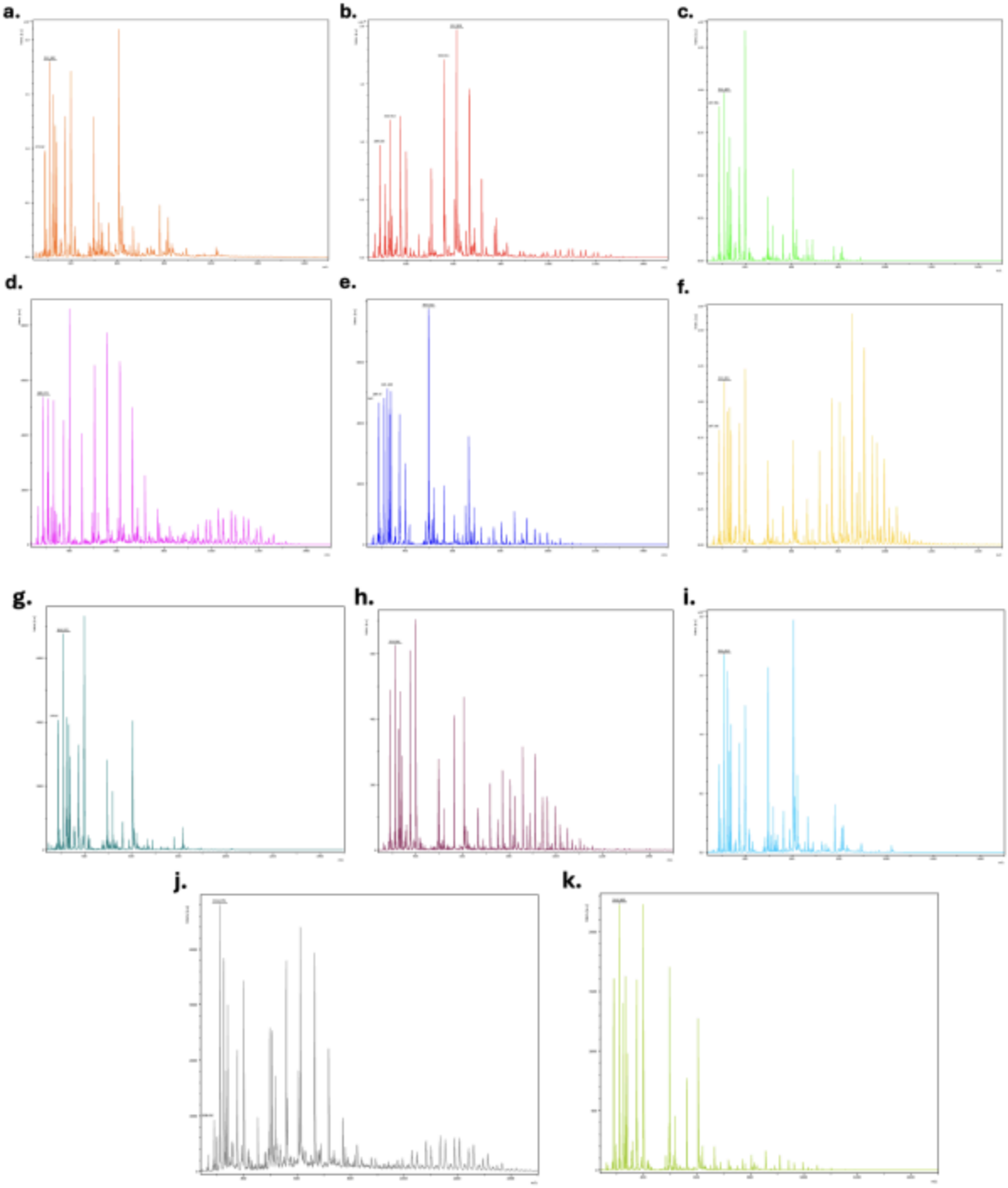
a.
b.
c.
d.
e.
f.
g.
h.
i.
j.
k.

2.7 Tables

Table 2.1 List of polymer types, vendors, and physicochemical characteristics. Comprehensive summary of polymers, vendors, densities (g/cc), molecular weight (g/mol), and physical properties, like texture and shape.

Polymer	Vendor	Density (g/cc)	Molecular Weight (g/mol)	Physical Form
Polystyrene	Cospheric	1.03-1.05	-	Spheres
Low Density Polyethylene	Cospheric	0.95-0.98	-	Spheres
Polystyrene	Scientific Polymer Products	1.06	1,200	Powder
Low Density Polyethylene	Scientific Polymer Products	0.92	50,000	Powder
Polyacrylonitrile	Scientific Polymer Products	1.184	150,000	Powder
Polycarbonate	Scientific Polymer Products	1.20	36,000	Pellet
Polysulfone	Scientific Polymer Products	1.24	60,000	Pellet
Nylon 6	Scientific Polymer Products	1.14	25,000	Pellet
Nylon 6(3)T	Scientific Polymer Products	1.12	-	Pellet
Nylon 6/6	Scientific Polymer Products	1.30	-	Pellet
Nylon 6/10	Scientific Polymer Products	1.08	15,000	Pellet
Nylon 11	Scientific Polymer Products	1.04	-	Pellet
Nylon 12	Scientific Polymer Products	1.02	-	Pellet
Poly(methyl methacrylate)	Scientific Polymer Products	1.20	15,000	Powder
Poly(vinyl chloride)	Scientific Polymer Products	1.40	130,000	Powder
Styrene/acrylonitrile copolymer	Scientific Polymer Products	1.07	185,000	Powder
Polyacrylonitrile	Sarchem Labs	1.184	70,000	Powder

Table 2.2. Select polymers for SEM imaging analysis. Polyacrylonitrile preps generated within one month of imaging were selected, diluted tenfold in pure EtOH or deionized water, and assembled on carbon tape after drying for ≥ 4 hours in the chemical fume hood.

Polymer	Prep ID	Vendor	Fragmentation Modality	Fragmentation Time (min)	Concentration (mg/mL)	Suspension Medium for Drying
Polyacrylonitrile	2H3	Scientific Polymer Products	Bath Sonication	90	25.50	Pure EtOH
Polyacrylonitrile	2H3	Scientific Polymer Products	Bath Sonication	90	25.50	Water
Polyacrylonitrile	2H1	Sarchem Labs	Bath Sonication	90	14.10	Pure EtOH
Polyacrylonitrile	RE1	Sarchem Labs	Bath Sonication	150	34.40	Pure EtOH
Polyacrylonitrile	BM1	Sarchem Labs	Bath Sonication	30	34.70	Water

Table 2.3. Preps generated for longitudinal observation of particle dynamics in solution. PAN preps were generated with 30 minutes of sonication according to Chapter 2, section 2.5.3, and size analyzed using DLS at time points listed in Chapter 2, section 5.2.8.

Polymer	Prep ID	Vendor	Fragmentation Modality	Concentration (mg/mL)
Polyacrylonitrile	L1	Scientific Polymer Products	Bath Sonication	24.75
Polyacrylonitrile	L2	Scientific Polymer Products	Bath Sonication	24.12
Polyacrylonitrile	L3	Scientific Polymer Products	Bath Sonication	33.77
Polyacrylonitrile	L4	Scientific Polymer Products	Bath Sonication	28.90
Polyacrylonitrile	L5	Scientific Polymer Products	Bath Sonication	37.50
Polyacrylonitrile	L6	Scientific Polymer Products	Bath Sonication	38.57

Table 2.4. Longitudinal analysis of size using the diameter of the most prominent population. Preps were analyzed via DLS using the protocols discussed in Chapter 2, section 2.5.4. Triplicate measurements for the most prominent population based on signal intensity were averaged and reported with standard deviation.

Prep ID	Concentration (mg/mL)	Day 0 (nm)	Day 7 (nm)	Day 14 (nm)	Day 31 (nm)	Day 35 (nm)	Day 43 (nm)	Day 59 (nm)
L1	24.75	288.7±5.00	650.1±6.81	549.8±12.6	715.03±48.4	421.4±11.7	313.5±7.30	440.5±1.62
L2	24.12	298.4±4.03	825.9±22.6	721.5±43.0	372.7±10.4	476.5±2.42	498.5±6.95	450.9±6.86
L3	33.77	219.1±10.5	483.7±19.0	525.4±2.84	426.8±8.40	459.8±9.05	530.8±16.3	307.9±10.2
L4	28.90	358.1±4.11	773±65.3	602.7±12.2	556.3±6.40	506.5±4.52	490.8±6.69	431.4±4.86
L5	37.50	342.9±4.24	1509±261	815.8±80.9	927.3±22.5	522.6±6.12	585±24.4	570.4±7.16
L6	38.57	238.2±0	954.6±0	643.8±0	467.1±0	502.5±13.7	519.7±8.58	No Measured Value

Table 2.5. Evaluation of endotoxin in plastic preps. Selected PAN solutions were diluted 1:1 and prepared according to vendor protocols, alongside controls. Optical density at 545 nm was measured as described in Chapter 2, section 2.5.9. LPS concentrations (EU/ML) were corrected with the water control. Per GenScript, 1 EU is equivalent to 0.1 ng of LPS.

Polymer	Prep ID	Prep Concentration (mg/mL)	Corrected LPS Concentration (EU/mL)
PAN	PAN B1	28.20	0.288
PAN	PAN B1 Rerun	34.30	0.333
PAN	PAN Y	26.70	0.200
PAN	PAN SM	25.50	0.132
PAN	PAN 1	24.80	0.239

Table 2.6. Evaluation of optical noise in microplastic preps for LAL test. PAN was prepared at 26.80 mg/mL and sonicated for 1 hour. The stock prep was tenfold serially diluted. Duplicate absorbance was measured at 545 nm in a 96-well plate.

Concentration	Average Optical Density	Standard Deviation (*n-1*)
1/10	0.74125	0.3200
1/100	0.1385	0.0124
1/1000	0.1241	0.0161
Blank	0.1176	0.0117

Table 2.7. Preparation of nonsterile PAN preps for analysis of sonication parameters. SPP PAN was resuspended in an aqueous solution and sonicated for varying times, at different locations, and using varying bath volumes and temperatures to assess the effects of heat transfer, energy density, and bath volume.

Prep ID	Fragmentation Modality	Time (min)	Location in Sonicator	Sonicator Volume (mL)	Concentration (mg/mL)	Temperature (°C)
I10a I10b	Sonication	15, STOP, 15	Middle	1000	26.3 25.61	Room
I11a I11b	Sonication	15, STOP, 15	Corner	1000	26.01 25.03	Room
I16 I17	Sonication	15	Corner	1000	24.23 24.9	Room
I18 I19	Sonication	15	Middle	1000	21.83 27.34	Room
I20 I21	Sonication	15	Corner	500	22.07 24.66	Room
I22 I23	Sonication	15	Middle	500	27.05 23.87	Room
C1X	N/A	N/A	N/A	N/A	25.21	Room

Table 2.8. Prep size following parameter variation. Duplicate preps prepared at similar concentrations were measured per Chapter 2, section 2.5.4, with three replicate measurements per prep averaged. The Z-average diameter and the diameter of the population with the greatest signal intensity were recorded.

Prep ID	Z-average diameter (nm)	Diameter of Largest Peak (nm)
I10a I10b	182.0 211.8	201.8 219.2
I11a I11b	659.2 1045	647.8 637.3
I16 I17	845.1 294.0	682.4 309.8
I18 I19	389.7 193.5	393.5 213.5
I20 I21	1051 1315	644.0 476.0
I22 I23	169.0 170.3	181.0 177.2
C1X	2090	3536

Table 2.9. DLS analysis of unsonicated polymers suspended in DI water. Preps were weighed and resuspended in 1 mL of DI water in preparation for DLS size analysis.

Prep ID	Polymer	Concentration (mg/mL)	Z-average diameter (nm)	Diameter of Largest Peak (nm)
PAN NS	PAN	23.80	2099.83	1452.17
PMMA NS	PMMA	29.70	766.58	771.55
PVC NS	PVC	36.10	1437.83	1165.60
SP1	SAN	29.10	603.37	535.03
SAR 2	PAN	29.30	1826.0	1052.57
NSPP	PAN	28.20	2174.33	1125.67

CHAPTER 3: ESTABLISHING INDUCIBLE INFLAMMATORY RESPONSE *IN VITRO*

3.1 Introduction

The mammalian immune system is categorized into two functional responses: innate and adaptive. Innate immunity provides non-pathogen-specific protection of the host organism through canonical immunogenic molecules such as lipopolysaccharide (LPS) and mannose. Cells of the innate immune system include monocytes and more differentiated populations, such as macrophages and dendritic cells, as well as granulocytes, including eosinophils, neutrophils, and basophils. Innate immune cells originate in the bone marrow as hematopoietic stem cells, which mature into myeloid progenitors that further differentiate into monocytes, macrophages, and dendritic cells in response to environmental cues. These cells express a variety of molecules involved in antigen presentation and self-recognition, and can phagocytose foreign substances and initiate tissue remodeling. Hallmark central inflammatory pathways, such as pathogen-associated molecular patterns (PAMPs), are mediated through toll-like receptors and the transcriptional factor NF-κB [17]. Cell-to-cell communication is enforced through cytokines such as TNF-α, IL-6, and IL-1 [12].

The adaptive immune system leverages innate immunity to drive antigen-specific responses that are slow, yet powerfully targeted and specific. B-cells and T-cells are of the lymphoid lineage that generate unique DNA sequences for receptors that recognize specific antigens. CD8+ T-cells target MHC-I complexes presenting intracellularly derived foreign proteins and tumor-specific antigens, while CD4+ T-cells mediate immunity through cytokine expression and MHC-II on antigen-presenting cells (APCs), such as macrophages. B-cells drive antibody production and participate in antigen presentation.

Antibodies are unique to individual antigens and epitopes, and mark, opsonize, and neutralize exogenous invaders [17].

The immune system is poised to respond to a variety of stimuli with varying degrees of speed and specificity. With the extent of environmental burden of micro- and nanoplastics, including discovery in human saliva, sputum, lungs, livers, breast milk, blood, and feces, there is interest in understanding the degree of biomolecular and biomechanical interactions, including transport, localization patterns, mechanical stress, endocytosis, accumulation, and activated (or suppressed) signaling pathways [18]. It is of particular interest to understand how highly regulated systems, such as immunity, respond to compounds with unique properties, such as insolubility, topographical diversity, and inertness, that lack canonical motifs (PAMPs and DAMPs) derived through coevolution.

To model innate immunity, RAW 264.7 macrophages, an adherent cell line derived from Abelson murine leukemia virus, were chosen. Cells were exposed to a variety of microplastics generated by sonication, microwaving, or mechanical mashing. TNF-α, a hallmark proinflammatory cytokine, was measured in cell supernatant using a TNF-α Sandwich ELISA (BioLegend; San Diego, CA). Flow cytometry was used to confirm and optimize expression profiles, while bulk RNA sequencing was performed on positive indications of stimulatory behavior.

3.2 Results

3.2.1 TNF-a expression in RAW 264.7 as a function of microplastic exposure

Preliminary optimization of experimental parameters, including dosage, with pre-manufactured PS beads yielded no significant increase in TNF-α with respect to the vehicle. The positive control induced a measurable increase, with the highest concentration of PS at 1,200 µg/mL showing an elevated expression with larger variance between replicates. With preps at 30, 300, 500, 750, 900, and 1,200 µg/mL, actual concentrations in culture (at a 20 µL vehicle volume) were 2.4, 24, 40, 60, 72, and 96 ug/mL, respectively (Fig. 3.2). The commercially available PS beads had known concentration; we do not know the concentration of the soluble portion of the plastic preps. Notably, many preps had visible macroscopic insoluble particles when suspended in water at concentrations of 14-40 mg/mL. Thus, we surmise the maximum concentration of the microplastics is 40 mg/mL, but it is likely that a far smaller fraction actually is soluble at room temperature. Considering this, cells were treated with unique polymers exposed to a diverse set of fragmentation modalities (Fig. 3.3 and Table 3.1). PS sonicated for 1 and 1.5 hours, including a 2-minute microwave with 1.5-hour sonication, induced no measurable increase in TNF-α across a serially diluted dosing. A similar observation was noted in PA 6/12 preps sonicated for 30 minutes, 1 hour, and 2 hours, PA 12 sonicated for 30 minutes to 1 hour, and PA 6/6 sonicated for 30 minutes for stock to 100-fold dilutions (Fig. 3.3e and 3.3f). However, PAN sonicated for 1 hour induced a meaningful increase in TNF-α at the highest concentration in two independent experiments, with PAN sonicated for 1.5 hours inducing elevated TNF-α at stock and a tenfold dilution. In culture, the relative concentrations of plastic were a maximum of 1.021 mg/mL for the 1-hour sonication and 9.68 mg/mL for 1.5-hour sonication at the highest dosage (and tenfold serially diluted from stock). In a separate

experiment, PAN sonicated for 30 minutes, 1 hour, and 2 hours showed no significant elevation of TNF with respect to the control, despite an observed slight elevation (Fig. 3.3d). Estimated in-culture concentrations of plastics at the highest dosage were a maximum of 1.984 mg/mL, 1.792 mg/mL, and 1.784 mg/mL, respectively. Again, these are estimates of the quantity of insoluble polymer added to water, and the soluble microplastic and additional particulate concentration is not known. Relative elevations of TNF-α in LPS and water wells were expected and observed.

3.2.2 Observing no TNF-a output under similar dosing conditions

In three independent experiments, utilizing PAN sonicated for 1 hour diluted from stock to ten thousand-fold the concentration, as well as PVC and PMMA sonicated for an hour, and PMMA microwaved for 2 minutes, recorded TNF-α below the lower detection limit of the assay in both water and microplastic conditions. LPS generated a strong TNF-α response (Fig. 3.4a-c). Updated experimental protocols attempted a co-incubation of LPS and microplastic stimuli. At the largest dosage of 2.072 mg/mL with 1,500 ng/mL LPS priming, TNF-α yielded positive and significant induction over the LPS control from a PAN prep sonicated for 1 hour and mechanically mashed for 1 minute. TNF-α increased in a confirmatory experiment (Fig. 3.4d and 3.4e). When optimizing the positive control, significant elevations in TNF-α occurred again in the highest dosage of the plastic used in the previous experiment, with 150 ng/mL and 15 ng/mL LPS showing quantitatively greater TNF-α secretion over their respective controls (Fig. 3.4f). Additional analysis in scaled 6-well plates yielded similar results, with a PAN prep sonicated for one hour and mashed for 1 minute at a 2.144 mg/mL dosing impacting TNF-α output positively at 150 ng/mL LPS priming, with no measurable response in water or microplastic-only

conditions (Fig. 3.5a). Cell density was increased, and TNF-α was measured in conjunction with RNA collection for bulk RNA sequencing. A PAN prep sonicated for one hour and mashed for 1 minute at 2.144 m/mL in culture produced an observed TNF-α response, with measurable water and microplastic-only response (Fig. 3.5b).

3.2.3 Transcriptional signaling programs in RAW 264.7 cells

Microplastics induced a considerable upregulation in certain molecular programs. A dotplot illustrates a large proportion of differentially expressed genes from the blood remodeling pathway, with large numbers of genes in angiogenic and hypoxic pathways, enriched (Fig. 3.6a). A ridgeplot showed enrichment of these pathways in the microplastic condition, with a normal distribution of related genes from the previously stated pathways (Fig. 3.6c). A dotplot for the LPS condition displayed discrete upregulation in programs related to ribosome biogenesis, response to biotic stimulus, and response to LPS (Fig. 3.6d).

3.3 Discussion

We observed that RAW 264.7 produced a limited and non-significant response to polystyrene during the MP and NP optimization experiment (Fig. 3.3a). In subsequent experiments, TNF-α was consistently and significantly induced by SPP PAN at two distinct concentrations (Fig. 3.3b and 3.3c). In a review by Bianchi et al., TNF-α (and other M1 cytokines) were meaningfully upregulated by PTFE and PS, with hybrid M1/M2 phenotypes reported [19]. Pro-inflammatory responses are well-reported in the literature across numerous cell types and polymers. Interestingly, in future experiments, PAN and other polymers induced TNF-α below the lower detection limit of the assay, with the LPS condition producing a strong response (Fig. 3.4a-c). It was hypothesized that the lack of response in these cells was a

phenotypic shift from the previously thawed population, in that the macrophage basal activation was a prevailing M0 state. To reinduce an inflammatory state, LPS was co-incubated with PAN. In co-incubated conditions, TNF-α was significantly induced over the baseline LPS output (Fig. 3.4d and 3.4f). The introduction of LPS not only reintroduced the cells to their previously observed basal activation, but it also primed them into a canonical state of pro-inflammatory activity, characterized by cytokine release, phagocytosis, and antigen presentation. In a study by Liu et al., mice expressing acute ulcerative colitis were generated and fed polystyrene microplastics. After MPs, the UC-induced mice exhibited enhanced immune dysfunction with increased pro-inflammatory cytokine expression [20]. Immune dysfunction poses an interesting challenge, as our data strongly suggest the state of the cells, especially when activated, amplifies localized inflammation and potential damage to the surrounding tissue when exposed to microplastics. Those who exhibit pro-inflammatory conditions are likely more susceptible to microplastic burden.

In the PAN-stimulated condition, transcriptional signaling indicated upregulation of distinct programs involving angiogenesis, blood vessel remodeling, and hypoxia. Gene ontologies for differentially expressed genes, such as *PLK2*, *IL1RN*, *CCL4*, *ANPEP*, *Gpnmb*, and *Ndrg1*, describe positive regulation of the cell cycle, IL-1 antagonism, antimicrobial immune responses, tissue remodeling, negative regulation of inflammation, and response to hypoxia, respectively. Versus the vehicle control, microplastics induced a state of cell growth (cell cycle), tissue expansion (angiogenesis), and reduction in inflammation, all characteristics consistent with a wound-healing, M2-like phenotype. Interestingly, *CCL4* was preserved as a pro-inflammatory gene involved in leukocyte chemotaxis, which was observed in the incubation of PS-NPs in measuring microglial activation [21]. The upregulation of gene sets related to

hypoxia is a compelling result that begs an investigation into concentration-induced stress. With particles of varying sizes and morphologies, the existence of M2-like signaling programs and hypoxia suggests damage (or extreme stress) to cells and activation of DAMPs, or damage-associated molecular patterns. Confirmatory assessment of true M1 activation was performed in the LPS condition, which indicated positive enrichment of cellular responses to LPS, generalized immune cell chemotaxis, and response to a biotic stimulus (Fig. 3.6).

3.4 Methods

3.4.1 Preliminary optimization of culture conditions for TNF-a release

Standard CR-10 media was prepared from RPMI 1640 with L-glutamine, 10% heat-inactivated fetal bovine serum (FBS), 1% penicillin/streptomycin, sodium pyruvate (200 mM), non-essential amino acids (NEAA), L-glutamine (200 mM), 0.5% sodium bicarbonate (7.5% w/v), and 0.1% 2-mercaptoethanol (55 mM) (Gibco; Waltham, MA). Cryopreserved RAW 264.7 cells were thawed in a 37°C bath for two minutes, and then slowly dispensed into 9 mL of warmed CR-10 and spun at 500 g for 5 minutes (Eppendorf; Enfield, CT). The media was decanted into 10% bleach, and cells were resuspended in 10 mL of warmed CR-10. Then, a T75 or T175 flask (depending on required surface area) was inoculated with the prepared suspension and incubated at 37ºC and 5% CO_2 (Gibco; Waltham, MA, USA).

Cells were monitored for overcrowding and viability and were passaged between 80 and 90% confluence with a 1x HBSS wash and 0.25% Trypsin/EDTA (Gibco; Waltham, MA, USA). During passaging, cells were counted with a glass hemocytometer, with a fraction seeded in a flat-bottom, 96-well plate in 250 uL of CR-10 at densities of 1,000, 5,000, and 9,000 cells per well (Corning; Corning, NY, USA) and incubated at 37ºC and 5% CO_2 for 4 hours. Afterward,

cells were stimulated with 1,500 ng/mL of LPS and incubated under the same conditions for 24 and 48 hours. Supernatants were collected post-stimulation and frozen at -80ºC.

3.4.2 Optimization of microplastic dosing in RAW 264.7 cultures

Using the thawing strategy, passaging protocol, and medium composition from Section 3.4.1, 2,000 cells were seeded at passage 20 in a flat-bottomed 96-well plate in 250 µL of medium. Polystyrene microspheres (Cospheric, LLC.; USA) with known diameters of 4.8 to 5.8 µm listed in Table 2.1 were prepared following the methods described in Section 2.5.3 to a final concentration of 22 mg/mL. Dilutions were prepared at approximate concentrations of 1,200, 900, 750, 500, 300, and 30 µg/mL in culture. Cells were incubated at 37ºC and 5% CO_2 for 24 hours. Supernatants were collected at the end of the incubation period and frozen at -80ºC.

3.4.3 Stimulation of RAW 264.7 cells with MPs and NPs

Unless otherwise specified, all plastic stimulation experiments were performed using the culturing protocols and experimental groups described in this section. Using the thawing strategy, passaging protocol, and medium composition from Section 3.4.1, 2,000 to 2,500 cells were seeded in a flat-bottom 96-well plate in 250 uL of complete medium. Cells were allowed to settle for ≥ 30 minutes.

Next, plastic preps generated according to Sections 2.5.2 and 2.5.3 were aliquoted into 1.5 mL Eppendorf tubes in the sterile hood. Two to four tenfold serial dilutions of plastic were prepared by allowing the larger plastics to sediment and agitating to resuspend smaller particles into the upper fraction of liquid, which was removed and resuspended in deionized, sterile water (Gibco; Waltham, MA, USA). Stock concentrations of each prep were treated as estimates, as the

stock prep was not fully homogeneous for pipetting efficiency. After the cell settling period, preps were added in triplicate to culture in 20 µL volumes to prevent overdilution of the medium. 1,500 ng/mL LPS was prepared in culture from 50 µg/mL stocks in sterile, deionized water (Gibco; Waltham, MA, USA). 20 µL of sterile, distilled water was supplied as the vehicle control. Cells were incubated at 37°C and 5% CO_2 for 12 to 24 hours. Supernatants were collected after incubation and frozen at -80ºC.

3.4.4 Inclusion of LPS as co-stimulatory molecule

For joint LPS and plastic stimulation, an LPS stock was generated at a working concentration of 18.75 µg/mL and 10x serially diluted to achieve concentrations of 1.875 and 0.1875 µg/mL. 20 uL were added to the experimental wells to achieve final concentrations of 1,500, 150, and 15 ng/mL in 250 uL of complete media. 18.75 µg/mL of LPS alone was added to wells as the positive control, while 20 uL of sterile, distilled water was incorporated for the microplastic-only and vehicle control wells. Cells were incubated at 37ºC for ≥ 30 minutes.

Following the initial incubation period, 20 µL from each well was removed. Plastic dilutions were prepared according to Section 3.4.3 and supplied in triplicate across wells possessing the established LPS gradient and LPS-free wells. Wells not containing microplastics were supplemented with 20 uL more of DI water (Gibco; Waltham, MA, USA). Cells were incubated at 37ºC for 20 to 24 hours. After incubation, supernatants were collected and frozen at -80ºC.

Culturing conditions were scaled according to experimental need. For six-well plates, 36,000 to 200,000 cells were seeded in 3 mL of complete media per well (Corning; Corning, NY), with vehicle volumes scaling to 240 µL.

3.4.5 Enzyme-linked immunosorbent assay (ELISA) of supernatants

The TNF-α ELISA MAX Deluxe kit (BioLegend; San Diego, CA, USA) was used following the manufacturer's protocols for all microplastic stimulation experiments. 100 µL of coating buffer was prepared with anti-TNF-α capture antibody and incubated in a NuncSorp 96-well plate at 2-8ºC (Thermo Fisher Scientific; Waltham, MA, USA). All steps before substrate addition were performed at room temperature on a plate shaker (Thermo Fisher, *Clinical Shaker*; Waltham, MA, USA). Before addition of new reagents, 300 µL of wash buffer (1x PBS and 0.025% Tween 20) was added to wells, removed, and resupplied 4 times. 100 µL of stock supernatants were added in duplicate to the plate for culture conditions containing ≤ 10,000 cells and agitated on a plate shaker for 2 hours. Anti-TNF-α detection antibody was added and incubated for 1 hour. 100 µL of Avidin-Horseradish Peroxidase (AV-HRP) was added per well and incubated for 30 minutes. 100 µL of substrate solution was added per well and incubated in the dark for 15 minutes undisturbed. The reaction was terminated using 100 µL of acid per well. The plate was read at 450 and 570 nm (Molecular Devices, *VersaMax* or *SpectraMax M2* Plate Reader).

3.4.6 Bulk RNA sequencing of co- and monostimulated RAW 264.7 cells

Cells were seeded and stimulated for 24 hours in duplicate in a flat-bottomed 6-well plate per section 3.4.4. Supernatants were collected and frozen at -80ºC. The TNF-α ELISA MAX Deluxe kit was used following the manufacturer's protocols. Cells were then lifted by scraping and resuspended in 1.5 mL of CR-10 media. Once decanted, cells were treated for RNA extraction using the RNeasy Mini Kit (Qiagen; Hilden, Germany) and quantified via absorbance

at 545 nm in distilled, Ultrapure water (*NanoDrop*, Thermo Fisher Scientific; Waltham, MA, USA).

3.4.7 Statistical analysis

Four-parameter logistical (4PL) standard curves were generated according to the ELISA manufacturer protocol in GraphPad Prism version 11.0.2 (*GraphPad Prism*; Boston, MA, USA). Experimental group comparisons were performed by ordinary one-way analysis of variance (ANOVA) with Tukey's multiple comparisons test. Pairwise significance was determined at $p \leq 0.05$. Brown-Forsythe (BF) was performed for equivalent variance testing, with Welch's ANOVA performed when BF's $p \leq 0.05$, or group-to-group variance differed significantly. Experimental groups with replicates all below the lower detection limit and unavailable for interpolation by 4PL regression were omitted from the analysis.

For bulk RNA sequencing, STAR 2.7.1a aligned the reference genome. The DeSeq2 package was used for differential expression analysis, followed by a gene set enrichment analysis (GSEA) with genes ranked by log fold change (logFc).

3.5 Figures

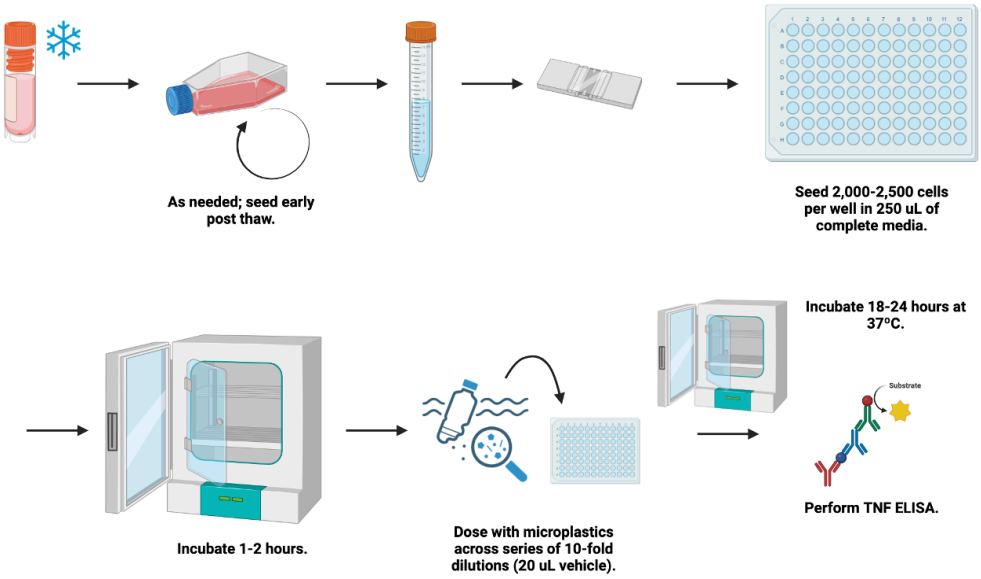

Figure 3.1. Culturing and dosing protocol for microplastic stimulation. RAW 264.7 cells were maintained in T75 culture flasks and passaged every 2 to 3 days. Cells were seeded at 2,000 to 2,500 cells per well in a 96-well plate and dosed with microplastics with the desired fragmentation criteria. A TNF-α ELISA was performed to quantify pro-inflammatory expression.

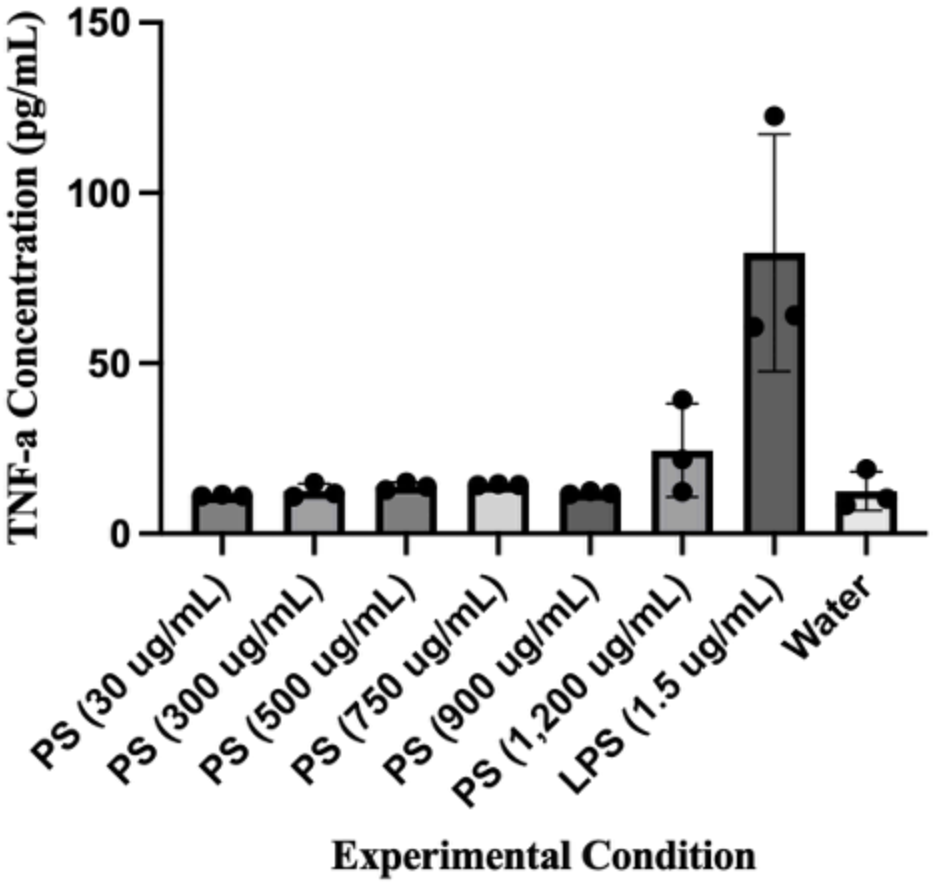

Figure 3.2. Microplastic stimulation optimization in RAW 264.7 cells. 2,000 RAW 264.7 cells per well were incubated with pre-manufactured PS microplastic beads between 4.8 and 5.8 µm for 24 hours. Supernatants were collected, and a TNF-α ELISA was performed. Corrected absorbance values at 450 nm were interpolated using a 4-parameter logistical regression and analyzed for significance with a one-way ANOVA and post hoc Tukey's test. *$p < 0.05$, **$p < 0.01$, ***$p < 0.001$, ****$p < 0.0001$. No significant differences ($p \leq 0.05$) were observed among the microplastic populations and the vehicle control.

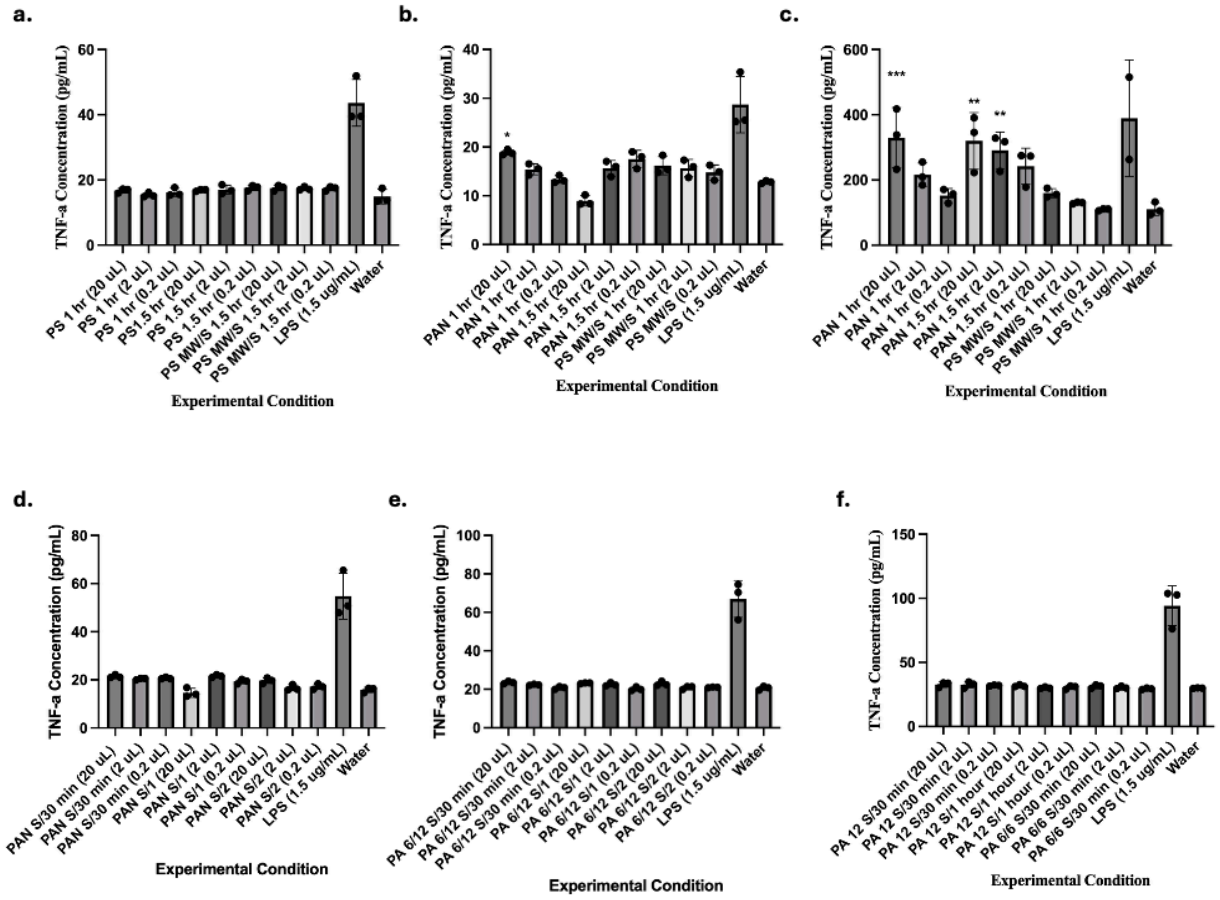

Figure 3.3. Multi-polymer incubation with RAW 264.7 cells and evaluation of TNF-α secretion. TNF-a values above were from wells seeded with 2,000 to 2,500 cells in a flat-bottom 96-well plate in 250 µL of complete RPMI and stimulated for approximately 1 day with 20 µL vehicle and 1.5 µg/mL LPS. **(a)** Incubated with the PS sonicated for 1 to 1.5 hours, with additional preps microwaved for 2 minutes. **(b)** Incubated with PAN sonicated for 1 to 1.5 hours with PS sonicated for 1 hour and microwaved for 2 minutes at a larger seeding density. **(c)** Repeat of conditions described in Figure 3.3b. **(d)** Incubated with PAN sonicated for 0.5, 1, and 2 hours. **(e)** Incubated with PA 6/12 sonicated for 0.5, 1, and 2 hours. **(f)** Incubated with PA 12 sonicated for 0.5 to 1 hour and PA 6/6 sonicated for 0.5 hours. Significance was determined via a one-way ANOVA with a post hoc Tukey's test or a Welch's ANOVA with Brown-Forsythe, as discussed in Chapter 3, section 3.4.7. *$p < 0.05$, **$p < 0.01$, ***$p < 0.001$, ****$p < 0.0001$.

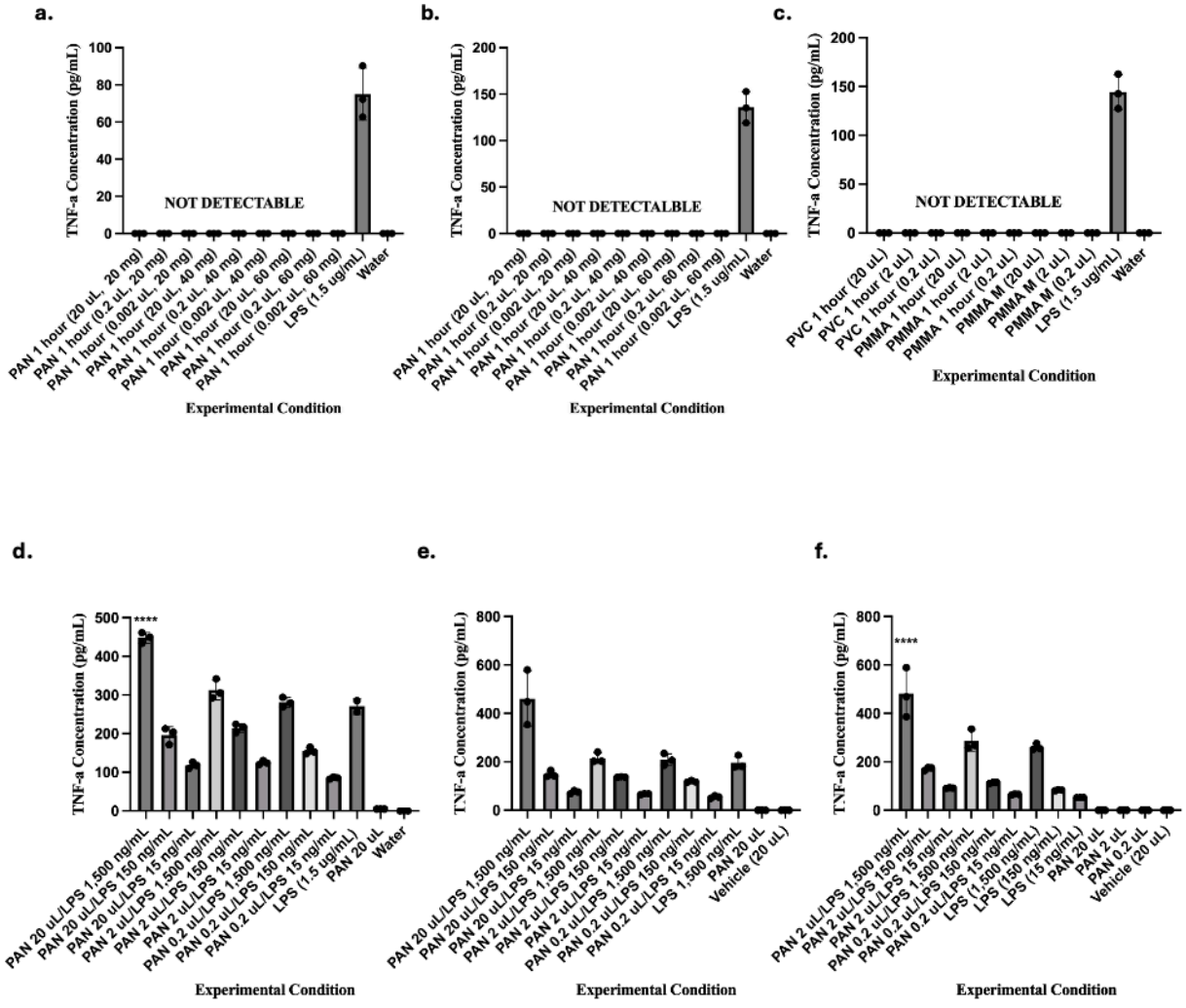

Figure 3.4. Continued measurement of TNF-α secretion following micro- and nanoplastic incubation, including observation of non-detectable signal and development of co-incubation scheme for inflammatory priming. TNF-a values listed above were from cells seeded at 2,000 to 2,500 per well in a flat-bottom 96-well plate in 250 µL of complete RRMI and stimulated for approximately 1 day with 20 µL vehicle and 1.5 µg/mL LPS at 37ºC and 5% CO_2. Priming with LPS occurred ≥ 0.5 hours before co-culturing with plastic **(a)** Incubated with PAN at stock, 1/100, and 1/10,0000 the stock concentration of 50 µg/mL. **(b)** Incubated under the same conditions as shown in Figure 3.4a. **(c)** Incubated with PVC or PMMA sonicated for 1 hour and PMMA microwaved for 2 minutes. **(d)** Co-incubated with 100-fold serial dilutions of LPS and PAN from 1,500 µg/mL and the stock prep, respectively. **(e)** Incubated under the same conditions as shown in Figure 3.4d. **(f)** Incubated under the same conditions as shown in Figure 3.4d with updated LPS controls at 150 µg/mL and 15 µg/mL. Significance was determined via a one-way ANOVA with a post hoc Tukey's test or a Welch's ANOVA with Brown-Forsythe, as discussed in Chapter 3, section 3.4.7. *$p < 0.05$, **$p < 0.01$, ***$p < 0.001$, ****$p < 0.0001$

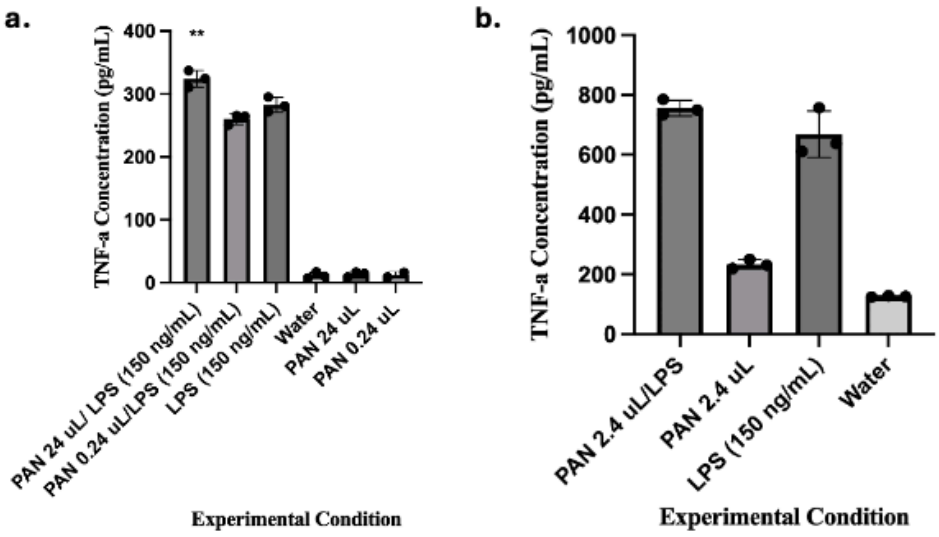

Figure 3.5. Increasing cell density to assess signaling impact and RNA extraction for bulk RNA sequencing. Cells were cultured in 6-well plates in 3 mL of complete RMPI media at 36,000 and 300,000 cells and incubated for 1 hour before co-culturing with plastic at a vehicle volume of 240 µL. Stimulation occurred for 20 hours at 37ºC and 5% CO_2. **(a)** 36,000 cells were cultured with PAN at a 10- and 100-fold dilution from stock, alongside LPS at 150 ng/mL. **(b)** 300,000 cells were cultured with PAN at a 100-fold dilution from stock, alongside LPS at 150 ng/mL. Results from DGE analysis are described in Fig. 3.6. Significance was determined via a one-way ANOVA with a post hoc Tukey's test or a Welch's ANOVA with Brown-Forsythe, as discussed in Chapter 3, section 3.4.7. *$p < 0.05$, **$p < 0.01$, ***$p < 0.001$, ****$p < 0.0001$.

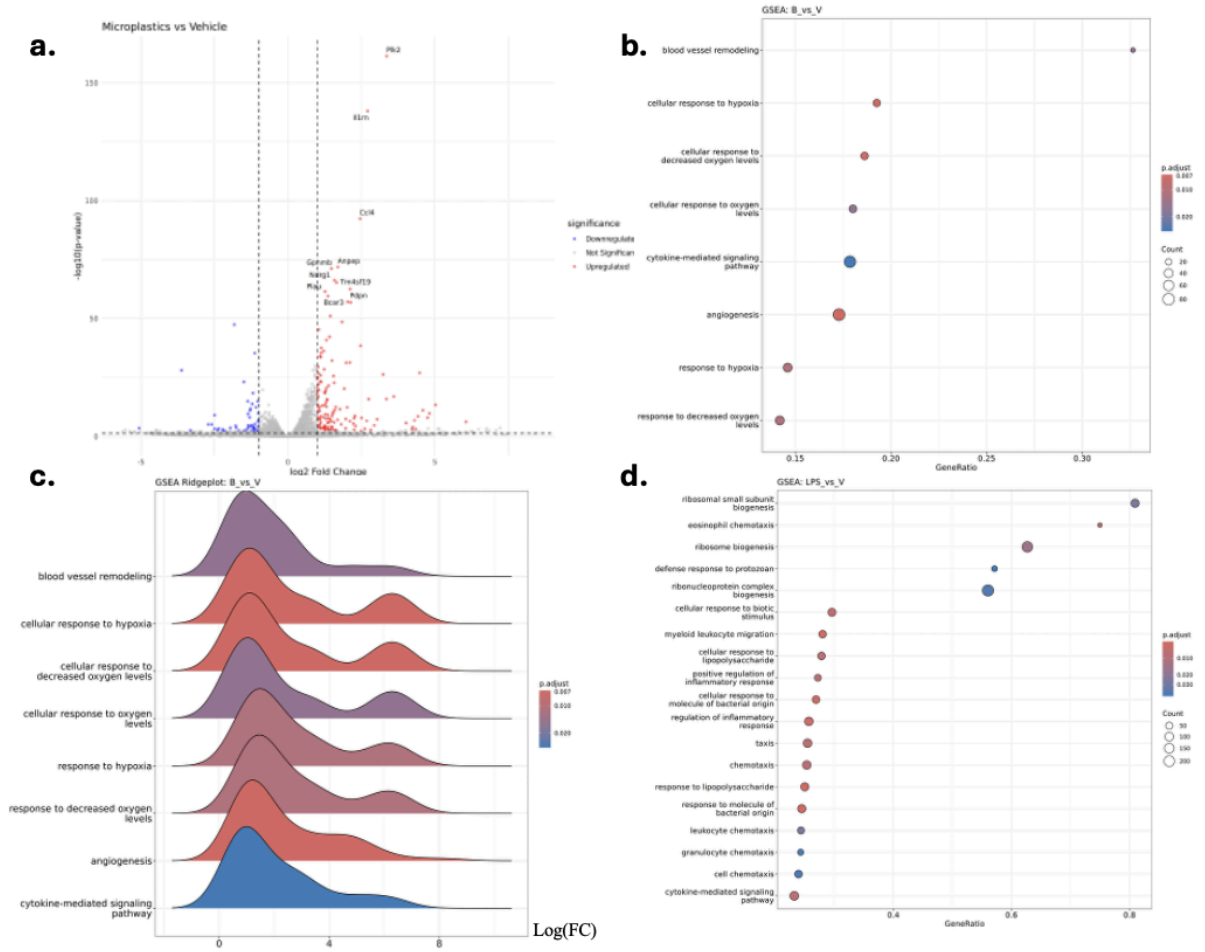

Figure 3.6. Differential gene expression (DGE) and gene set enrichment analysis (GSEA) of microplastic, LPS, and control conditions in RAW 264.7 cells. (a) Volcano plot ordering genes by adjusted p-values (-log10; listed as p-values) and log2 fold change in PAN microplastic (red) versus water (blue), with threshold for significance marked by > 1 log2 fold change and 50 for -log10 (p-value). **(b)** Dotplot GSEA representation for enriched pathways in the microplastic condition, including blood vessel remodeling, angiogenesis, and hypoxia. Gene ratio indicates the percentage of genes, a fractional representation of the pathway, from individual gene sets that are represented in the DEG list. Dot size indicates the number of genes from the pathway contributing to the enrichment score. **(c)** Ridgeplot illustration of gene upregulation in microplastic condition, as represented by spread of positive log fold change across each pathway. **(d)** Dotplot representation of enriched gene sets in LPS control; interpretation is identical to Figure 3.6b.

Table 3.1. Polymer types and preps incubated with RAW 264.7 cells. Preps listed below were size analyzed via DLS and incubated with RAW 264.7 cells utilizing varied experimental conditions. Preps listed with no measured value failed to meet minimum requirements for DLS.

Prep ID	Polymer	Fragmentation Modality	Time (min)	Concentration (mg/mL)	Z-average diameter (nm)	Diameter of Largest Peak (nm)
1	PAN	Sonication	30.00	24.80	481.7	520.7
2	PAN	Sonication	60.00	22.40	644.7	535.6
3	PAN	Sonication	120.00	23.30	435.9	469.2
PAN Sonication 1 hour	PAN	Sonication	60.00	12.76	350.9	385.8
PAN Sonication 1.5 hour	PAN	Sonication	90.00	121.00	No Measured Value	No Measured Value
PAN 20	PAN	Sonication	60.00	23.00	416.4	435.3
PAN 40	PAN	Sonication	60.00	47.00	429.5	462.7
PAN 60	PAN	Sonication	60.00	58.00	354.6	384.9
PS Son 1hr	PS	Sonication	60.00	15.21	459.4	436.8
PS Son 1.5hr	PS	Sonication	90.00	121.00	290.0	304.9
PS MW+Son 1 hour	PS	Microwave + Sonication	60.00	12.02	310.0	292.4
PS MW+Son 1.5 hour	PS	Microwave + Sonication	90.00	60.00	289.9	304.8
A1	PA 6/12	Sonication	30.00	18.00	No Measured Value	No Measured Value
A2	PA 6/12	Sonication	60.00	18.20	No Measured Value	No Measured Value
A3	PA 6/12	Sonication	120.00	18.00	No Measured Value	No Measured Value
Y1	PA 6/6	Sonication	30.00	23.00	No Measured Value	No Measured Value
X1	PA 12	Sonication	30.00	20.00	No Measured Value	No Measured Value
X2	PA 12	Sonication	60.00	25.90	298.7	517.4
X	PC	Sonication	60.00	18.00	No Measured Value	No Measured Value
B	PSU	Sonication	60.00	22.60	No Measured Value	No Measured Value
PVC 1	PVC	Sonication	30.00	25.30	2012.25	729.15
PMMA 1	PMMA	Sonication	30.00	20.80	394.95	555.05
PMMA M	PMMA	Microwave	2.00	17.70	657.9	705.3

CHAPTER 4: ASSESSING PHYSIOLOGICAL RELEVANCE WITH MURINE BONE MARROW DERIVED MACROPHAGES

4.1 Introduction

In vitro macrophage systems provide a discrete strategy for modeling innate immune function, including cytokine expression, antigen presentation, and phagocytosis. RAW 264.7 cells are a robust and scalable cell line that offers efficient insight into system physiology in mice and humans. The microplastic literature focuses heavily on cell lines for systems commonly in contact with particles, including the intestinal and pulmonary epithelia, and hepatocytes; specific cell lines include Caco, HepG2, and A549 [22]. Interestingly, fewer papers explore primary cell cultures as meaningful alternatives to cell lines. Bone marrow-derived macrophages (BMDMs) are a commonly used cell culture system for emulating macrophages *in vivo*. Cells are isolated from the femur and tibia of an immunocompetent mouse and cultured for 5 to 7 days in DMEM containing macrophage colony-stimulating factor (MCSF). This cytokine drives macrophage differentiation from hematopoietic stem cells. Genetically, BMDMs more closely resemble *in vivo* populations. A recent study performed by Moosavi et al. generated immortalized BMDMs and treated them with 1 ug/mL PS nanoplastics. They observed particle localization in the endoplasmic reticulum after endocytic uptake along with cytotoxicity. An elevation in ROS production was noted, particularly as an inflammatory mechanism. The authors emphasized both the elevation of the listed diagnostic markers and the marked sensitivity of BMDMs over cell lines [10].

Bone marrow-derived cells were chosen to establish a closer physiological relevance to the innate immune system, provide a more sensitive and stable model to discrete changes in

environmental stimuli, and validate findings from the RAW 264.7 model. Polymers generated through various fragmentation modalities were incubated with BMDMs overnight. To quantify pro-inflammatory upregulation, a TNF-α Sandwich ELISA was performed. Transcriptional profiles were generated through bulk RNA sequencing.

4.2 Results

4.2.1 Positive indications of TNF-α release in co-incubation of LPS and PAN

Using the co-incubation protocol from the RAW 264.7 model, BMDMs were stimulated with PAN preps with varying fragmentation characteristics. Two independent experiments displayed significant TNF-α versus the control, with two showing a strong elevation. Specifically, PAN sonicated for 1 hour and mechanically mashed for 1 minute was supplied to cells at 0.2744 mg/mL at the highest concentration and once tenfold serially diluted. The highest concentration of plastic was highly significant with respect to the control (Fig. 4.2a). The co-stimulatory conditions were significant at both stock and tenfold dilutions against 150 ng/mL, 15 ng/mL, and 1.5 ng/mL LPS (Fig. 4.2b-d). A duplicate experiment was performed, producing significant results in both the fully concentrated (2.744 mg/mL in-culture concentration) and tenfold diluted microplastic solo incubations (Fig. 4.2e). Culture conditions were scaled to a 24-well plate, and cells were treated with PAN sonicated for 30 minutes at an incubation concentration of 0.1942 mg/mL, with both the co-stimulation and microplastic-only conditions showing meaningful increases in TNF-α (Fig. 4.2f).

In an additional observation, using the PAN prep described in the previous experiment, PAN induced significant TNF-α induction at 15 ng/mL and 1.5 ng/mL LPS using a tenfold dilution of the stock prep, alongside the solo incubation of plastic; the largest prep concentrations in culture were 0.1942 mg/mL (Fig. 4.3a). SAN, a co-polymer comprised of alternating PAN and

SAN monomers, induced little to no elevation of TNF-α at the same previously listed dilution factors; the largest prep concentrations in culture were 0.1604 mg/mL (Fig. 4.3b).

Finally, BMDMs were exposed to a new PAN vendor, sterile-filtered plastics, unsonicated preps, and stimulations for RNA extraction and sequencing, with varied TNF-α response profiles. Following co-incubation of 15 ng/mL LPS with new PAN microplastic sonicated for 30 minutes at a ten- and 100-fold dilution against respective controls (0.2776 mg/mL at the highest concentration), TNF-α showed no statistically meaningful difference from respective controls (Fig. 4.4a). In preps that were size exclusion filtered for < 0.22 μm particles, a similar negative response was observed, with no measured concentration value post-filtration (Fig. 4.4d). Additionally, unsonicated PAN at a tenfold dilution (0.2346 mg/mL in culture) and PAN sonicated for six hours (0.2560 mg/mL in culture) were tested. The six-hour sonication induced an elevation of TNF-α, despite lack of statistical significance, with singular incubations of microplastic not enhancing a stimulatory effect (Fig. 4.4c). Finally, a prep generated with 1.5 hours of sonication at a 2.040 mg/mL culture dosage showed distinct increases in TNF-α in LPS-primed conditions, with negligible differences in the microplastic-only and vehicle conditions (Fig. 4.3b).

4.2.2 Transcriptional signaling in BMDMs

Three sets of conditions were compared: LPS and vehicle, MP and vehicle, and PAN + LPS and LPS. Utilizing normalized enrichment score, based on a ranked differentially expressed gene list, the LPS condition indicated upregulation of IFN-γ, IFN-α, TNF-α, and STAT-3, while downregulating angiogenesis and cholesterol homeostasis (Fig. 4.5a and 4.5b). In the co-incubation condition, IFN-γ and IFN-α were downregulated, with TNF-α preserved.

Additionally, angiogenesis and cholesterol homeostasis were upregulated (Fig. 4.5c and 4.5d). In the solo microplastic condition, the cytokine profile was similar to the LPS-priming condition, with gene sets comprising MYC Targets v1 and v2 upregulated, and generalized inflammatory responses downregulated (Fig. 4.5e-f).

4.3 Discussion

BMDMs produced similar, yet more consistently significant TNF-α responses over RAW 264.7 cells. At the highest experimental dosage, PAN induced a significant response over lower concentrations without the need for co-incubation with LPS, as found in RAW 264.7 cells (Fig. 4.2a). This indicated that primary BMDMs likely were already poised to respond to microplastics, whereas the RAW 264.7 cells typically required low-dose LPS-priming to respond to microplastics. Investigating the co-incubation conditions, PAN induced a strong elevation in TNF-α versus the LPS control (Fig. 4.2b-d). In MP-only conditions, TNF-α was upregulated (Fig. 4.2e and 4.2f). BMDMs exhibited a basal activation, a shift to an M1-like phenotype, evidenced by the measurable vehicle control. As described in the RAW 264.7 cells, this state is optimal for TNF-α induction, as the cells are already primed for inflammatory activity. Additional priming of macrophages into an elevated M1 state with LPS displayed similar elevations of TNF-α. These data (alongside RAW 264.7) suggest that macrophage responses to PAN are largely concentration-dependent, whether by means of cellular stress or receptor activation. Polymer chemistry was assessed with the introduction of SAN at a similar concentration and size, which induced little to no increase in TNF-*a* (Fig. 4.3a and 4.3b). Despite bearing the same nitrile group, SAN contains a large, alternating benzene moiety. Potential mechanisms of inaction include this functional group, or some distinct morphological or surface chemical difference.

Cells were treated with Sarchem PAN and displayed no measurable increase in TNF-*a*, along with the sterile-filtered preps and variation in prep characteristics between unsonicated and long sonicated preps (Fig. 4.4a and 4.4c). A lack of response to PAN obtained from the second vendor, despite the identical polymer chemistry, is compelling in that average diameter via DLS and SEM is the most prominent difference when compared to PAN obtained from SPP. Morphologically, Sarchem PAN is more rounded and porous. Thus, slight topographical differences could induce biomechanical stress by puncturing membranes. Furthermore, phagocytic potential, as Adler et al. observed, is dependent on MP concentration and size, as well as on the formation of ROS [23]. Finally, chemical contaminants between vendor sources could mediate the difference, as evidenced by spectral discrepancies in the FTIR readouts recorded previously (Fig. 2.5). Sterile filtration yielded an unresolvable response across the replicates, likely because prep concentrations were dilute. Therefore, filtered preps will require concentrating to assess inflammatory impact.

Transcriptional programs for the BMDMs trended similarly to RAW 264.7 cells. In the LPS-only condition, canonical M1 pathways were upregulated, including IFN-γ, IFN-α, and JAK-STAT-3, while tissue regeneration pathways were downregulated (Fig. 4.5b). When introducing PAN, the programming shifts sharply. The cells lose both IFN-γ and IFN-α enrichment, upregulate MYC targets, TNF-α, and exhibit an unfolded protein response (Fig. 4.5f and 4.4b). Not only does this contradict previous findings describing upregulation of numerous pro-inflammatory markers in other microplastic types, Schulze et al. describe MYC and its unique role as a master regulator of growth, tissue expansion, and angiogenesis. It is also a hallmark oncogene and massively upregulated in breast cancer, acting as a prognostic indicator of mortality [24]. Further analysis shows macrophage phenotypes are highly plastic and vary on

a spectrum across subtypes described in the literature as M1, M2, and M0. In an effort to delineate phenotypes, Jablonski et al. have described upregulation of *C-Myc* and *Egr2* as the most M2-centric genes, with *CD38*, *GPR18*, and *FPR2,* M1-centric [25]. Viewing normalized counts per million (CPM) in our BMDMs, *C-Myc* and *Egr2* maintained elevated expression in the microplastic-only condition, with those primed with LPS preserving *C-Myc* and *Egr2* over solely LPS (Fig. 4.5g). All facts considered, the described BMDMs strongly favor tissue remodeling pathways and preserve TNF-α, a conflicting hybrid phenotype suggesting macrophage dysregulation or a duration dependent shift to counterbalance a robust inflammatory start. Regardless, it seems macrophages aberrantly induce localized inflammation through TNF-α secretion, damage tissue, and signal for regeneration, a cycle primed for downstream implications involving prolonged inflammatory and oncogenic potential (Fig 4.5f). More compelling is the true anti-inflammatory potential of PAN in certain pathways. Even in the LPS co-incubation, PAN maintains the downregulation of IFN-γ and IFN-α, which are frontline cytokines in endotoxin-driven stimulation of the innate immune system (Fig. 4.5c and 4.5d).

4.4 Methods

4.4.1 Extraction and culturing of BMDMs

Bone marrow cells were harvested from the femurs and tibias of immunocompetent B6 mice by excising the legs and exposing the underlying bone through slow removal of the connective tissue with scissors and forceps. In the sterile hood, the bone caps were removed, and the marrow was extracted for 20 seconds at 10,000g in 1.5 mL Eppendorf tubes and resuspended in 100 uL of ice-cold PBS (Eppendorf; Hamburg, Germany). Cells were supplied with 4 mL of chilled ACK Lysis Buffer (Gibco; Waltham, MA) and incubated at room temperature for 6 minutes. Then, the suspension was passed through a 100 μm filter. Cells were seeded in a

24-well plate at 2,000,000 cells per well or a 96-well plate at 325,000 cells per well in 1 mL or 250 µL of DMEM supplemented with 10% heat-inactivated FBS, respectively. Cells were supplied with a 1:2000 dilution (25 ng/mL in culture) of macrophage colony-stimulating factor (MCSF) and incubated at 37°C and 5% CO_2. On day 3, cells were redosed with either 0.5 mL or 30 µL of MCSF-supplemented media at 25 ng/mL and incubated for four additional days. 1 mL or 250 µL of MCSF-free DMEM was refreshed on day 6 for improved visualization of the differentiated cells.

4.4.2 Stimulation strategy for BMDM exposure to micro- and nanoplastics

Specific stimulation parameters regarding scaling varied according to experimental need and are listed in Table 4.1. On day 8, cells planned for reseeding were washed with 1 mL of PBS and lifted with a cell scraper. Then, cells were seeded at 2,500 per well in a flat-bottom 96-well plate. Reseeded cells were allowed to settle for 4 hours. Cells unmoved from the maturation protocol remained in their original flat-bottom 24- or 96-well plates. Next, an LPS stock was generated at 50 µg/mL and supplied to achieve final concentrations of 150, 15, or 1.5 ng/mL in culture. Group stimulation strategy pre- and post-LPS addition followed Chapter 3, section 3.4.4, with cells incubated at 37ºC and 5% CO_2 for 15 to 120 minutes before microplastic introduction. After stimulation, cells were incubated for 12 to 24 hours at the same CO_2 and temperature conditions.

4.4.3 Enzyme-linked immunosorbent assay (ELISA) of BMDM supernatants

The BioLegend TNF-α ELISA MAX Deluxe kit was used following the manufacturer's protocols described in Chapter 3, section 3.4.5 for all microplastic stimulation experiments.

4.4.4 Bulk RNA Sequencing for BMDMs

Bone marrow cells were harvested from the femur and tibia of a female B6 mouse, seven months of age, and seeded in a 24-well plate at 2,000,000 cells per well in 1 mL of DMEM supplemented with 10% FBS, according to Chapter 4, section 4.4.1. On day 7, the old media was discarded, and an LPS stock was prepared at a working concentration of 50 μg/mL and serially diluted to 150 ng/mL. 1 mL was added to the experimental wells designated for plastic stimulation and others as the positive control. Vehicle-supplied, LPS-negative DMEM + 10% FBS was supplied to the microplastic-only and negative control wells. Cells were incubated at 37ºC and 5% CO_2 for 2 hours. Plastics listed in Table 4.2 were prepared at 1/100 of the concentration and incubated with cells at 8% of the culture volume, according to Chapter 3, sections 3.4.4 and 3.4.4. Cells were incubated at 37ºC and 5% CO_2 for 16 hours. After, cultures were treated per Chapter 3, section 3.4.6 with the Qiagen RNeasy Mini Kit and quantified using the NanoDrop.

4.4.5 Preparation of nanoscopic preps through sterile filtration

Bulk plastics were prepared according to Chapter 2, sections 2.5.2 and 2.5.3. Next, a 0.22 μm syringe-driven filter was primed with 100 μL of deionized water. Two preps with similar fragmentation characteristics were combined and mixed thoroughly in the sterile hood. Plastics were loaded into the syringe and slowly forced through the filter. After filtration, the membrane was washed with 100 μL of deionized water. BMDMs were stimulated with filtered preps for 2 hours during LPS priming and 24 hours for the longer incubation, according to Chapter 4, section 4.4.2. TNF-α concentrations were measured per Chapter 4, section 4.4.3.

4.4.6 Statistical analysis

Statistical analysis for the ELISA data was performed using GraphPad Prism version 11.0.2 per Chapter 3, section 3.4.7. Raw sequencing and pipeline analysis, including alignment, de-duplication, differential gene expression, and gene set enrichment analysis (GSEA), were performed according to technical documentation provided by Plasmidsaurus [26].

4.5 Figures

Figure 4.1. Extraction, differentiation, and stimulation protocols for bone marrow-derived macrophages. (a) Immunocompetent B6 mice were sacrificed according to the university ethics board and sprayed liberally with 70% EtOH. Skin and connective tissue were removed from both hind legs, which were then dislocated from the pelvic socket. Legs were washed with chilled PBS and cut at the ankle and the knee. 1.5 mL centrifuge tubes were prepared with 200 μL of chilled PBS, and 0.6 mL tubes were punctured with an 18G needle. Small cuts were made along the bone caps, and bones were loaded into the tubes and spun at 10,000g for 20 seconds. ACK Lysing buffer was supplied to remove residual RBCs, and cells were counted and plated at 2,000,000 or 300,000 cells per well in a 24- or 96-well plate. Cells were incubated for a week with 25 ng/mL MCSF in 1 mL or 250 μL of complete DMEM, with media replaced on day 3. (b) General protocol for microplastic stimulation under LPS-priming conditions in a 96-well plate. Cell densities and addition volumes were scaled between 24- and 96-well plates, as needed.

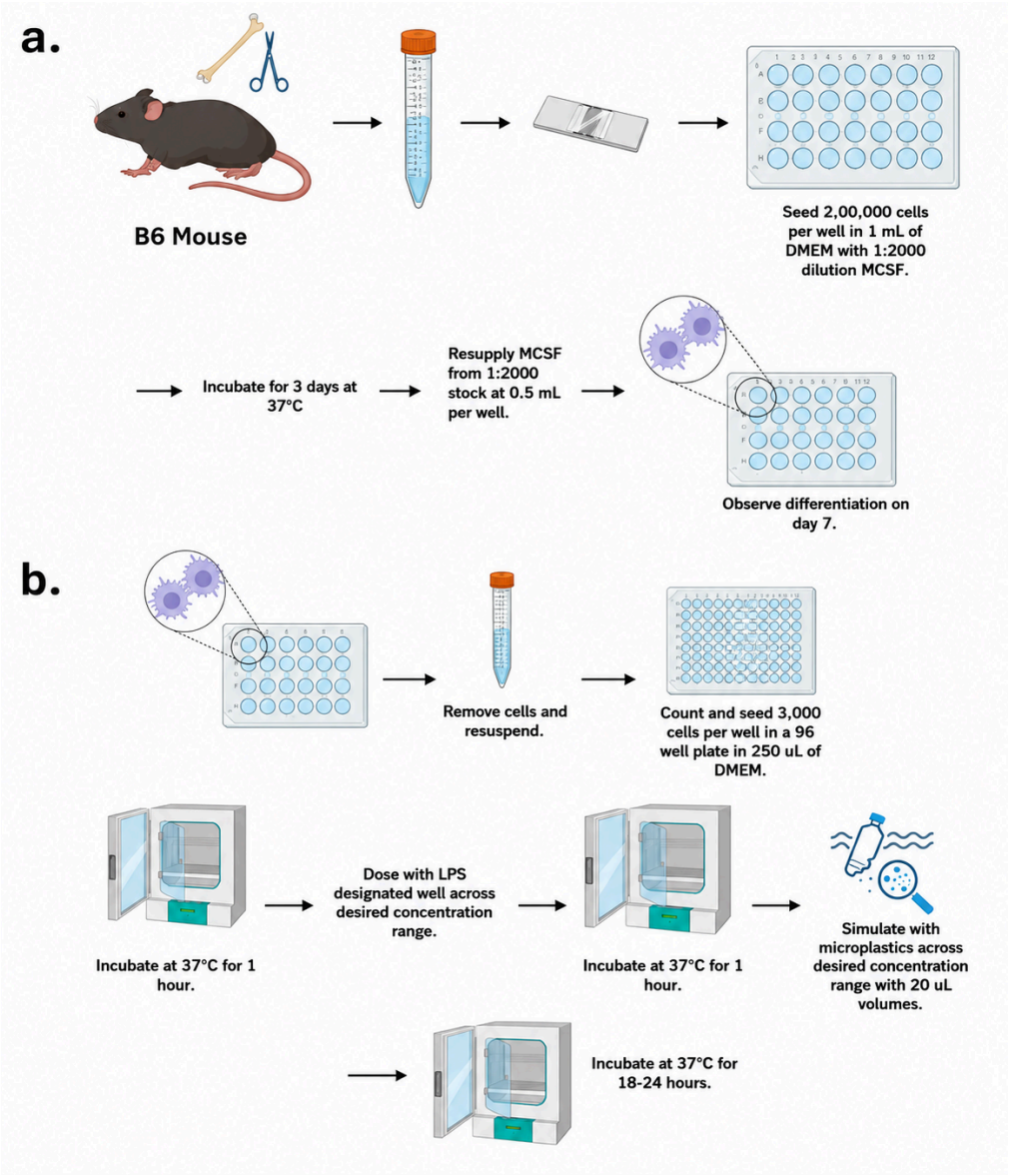
a.
B6 Mouse
Seed 2,00,000 cells per well in 1 mL of DMEM with 1:2000 dilution MCSF.
Incubate for 3 days at 37°C
Resupply MCSF from 1:2000 stock at 0.5 mL per well.
Observe differentiation on day 7.
b.
Remove cells and resuspend.
Count and seed 3,000 cells per well in a 96 well plate in 250 uL of DMEM.
Incubate at 37°C for 1 hour.
Dose with LPS designated well across desired concentration range.
Incubate at 37°C for 1 hour.
Simulate with microplastics across desired concentration range with 20 uL volumes.
Incubate at 37°C for 18-24 hours.

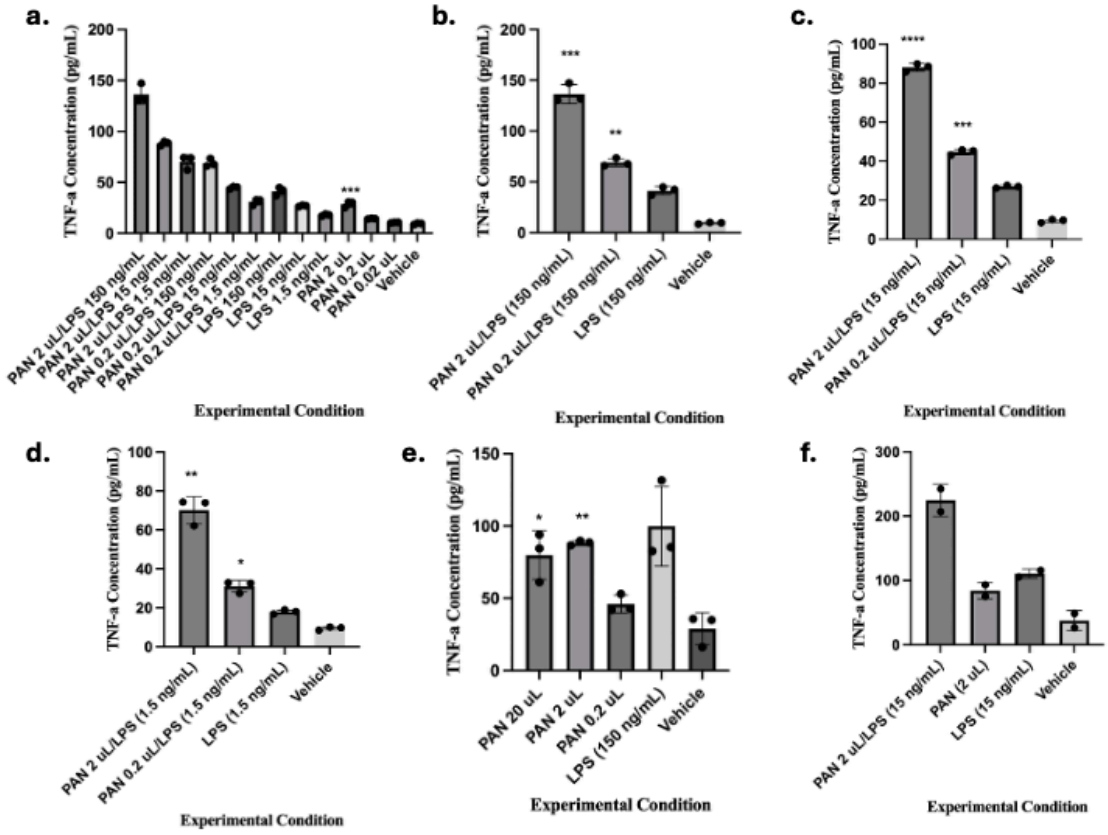

Figure 4.2. Culturing of bone marrow-derived macrophages with co-incubation of LPS and microplastic. After the 7-day differentiation protocol, BMDMs were removed and seeded in a flat-bottom 96-well plate at 3,000 cells per well. Cells were treated following the co-incubation protocol from Chapter 3, section 3.4.4. **(a)** Pilot treatment of BMDMs with ten-fold serial dilutions of LPS and microplastics from 150 ng/mL and stock. The significance indicator is with reference to the vehicle. **(b)** Comparison of PAN dilutions co-incubated with 150 ng/mL LPS against LPS control. **(c)** Comparison of PAN dilutions co-incubated with 15 ng/mL LPS against LPS control. **(d)** Comparison of PAN dilutions co-incubated with 1.5 ng/mL LPS against LPS control. **(e)** Introduction of BMDMs to PAN as a singular stimulatory component. **(f)** 30,000 cells were seeded per well in a 24-well plate and treated with PAN and positive/negative controls. Significance was determined via a one-way ANOVA with a post hoc Tukey's test or a Welch's ANOVA with Brown-Forsythe, as discussed in Chapter 3, section 3.4.7. *$p < 0.05$, **$p < 0.01$, ***$p < 0.001$, ****$p < 0.0001$.

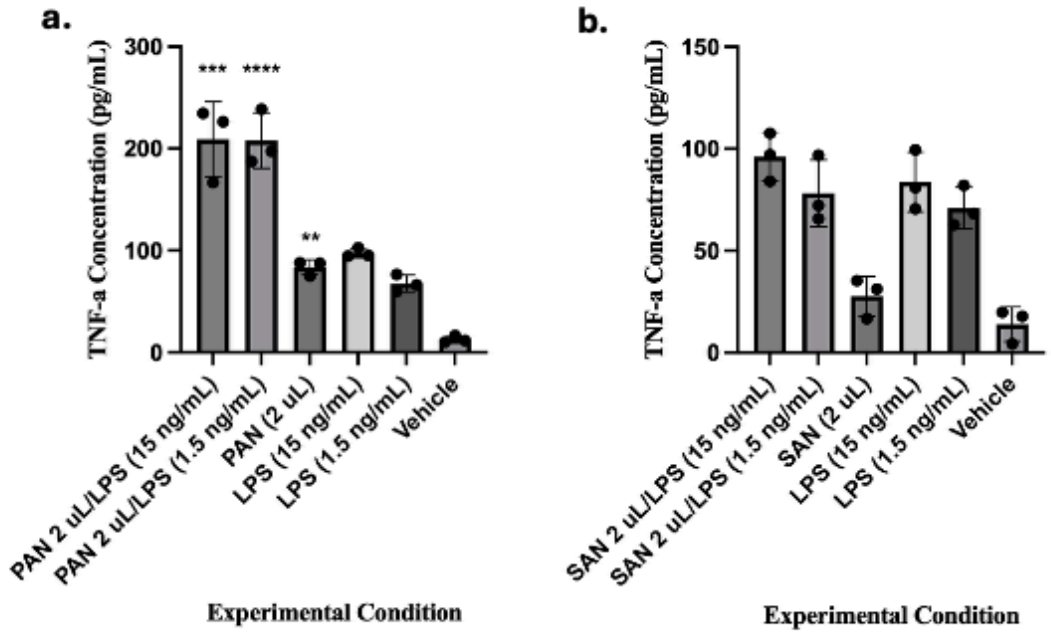

Figure 4.3. Inflammatory response to PAN and SAN, a structurally similar copolymer. 325,000 cells were seeded in 250 µL of complete DMEM in a flat-bottom 96-well plate and treated at 15 and 1.5 ng/mL LPS for 1 hour. **(a)** The polyacrylonitrile and **(b)** styrene acrylonitrile preps were serially diluted 10-fold from a stock solution. Then, microplastics were added in triplicate across wells with the previously established LPS gradient, as well as LPS-free and PAN wells. Cells were incubated at 37ºC and 5% CO_2 for 16 hours. Significance was determined via a one-way ANOVA with a post hoc Tukey's test or a Welch's ANOVA with Brown-Forsythe, as discussed in Chapter 3, section 3.4.7. *$p < 0.05$, **$p < 0.01$, ***$p < 0.001$, ****$p < 0.0001$.

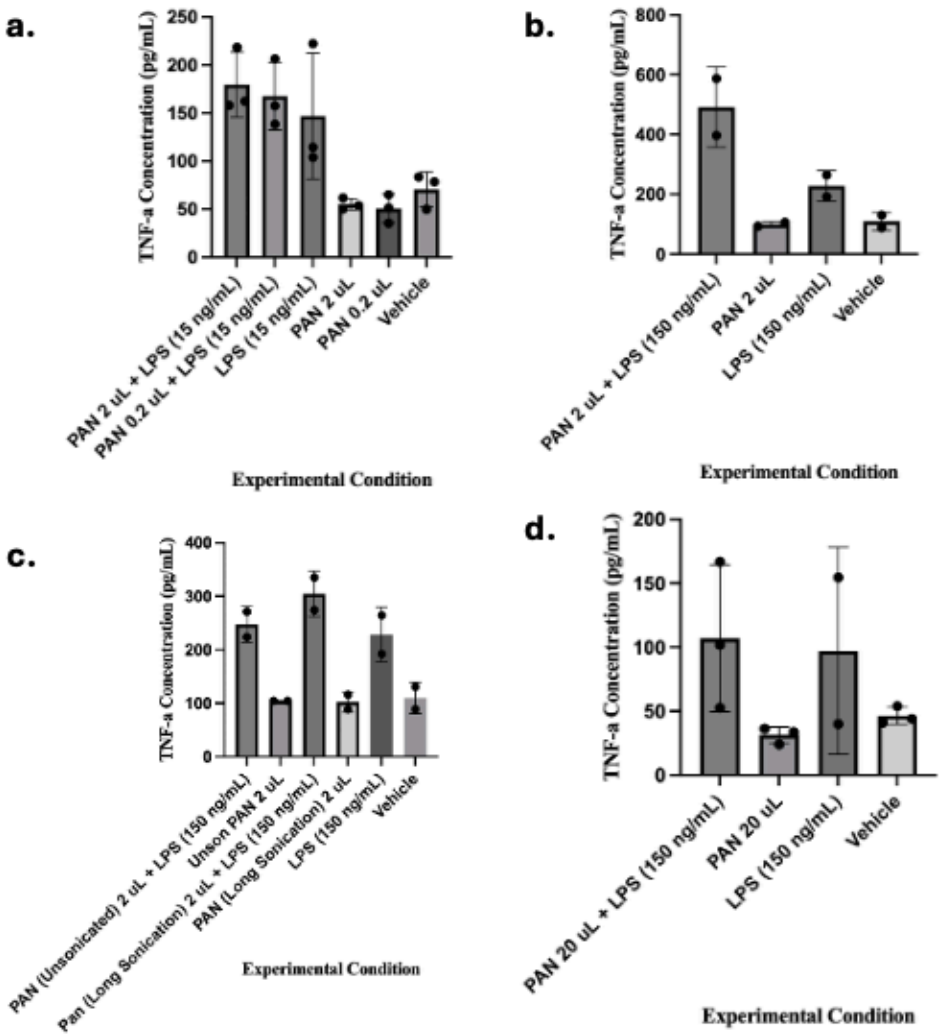

Figure 4.4. Cytokine response to PAN from different vendor, sterile-filtered plastics, and unsonicated preps and transcriptional signaling with original vendor incubation. (a) BMDMs were supplied with either DMEM and a vehicle control or DMEM containing 15 ng/mL LPS. Cells were incubated at 37ºC and 5% CO_2 for 15 minutes. Once 15 minutes elapsed, 100 µL was removed from each well. Then, the working concentration for the sonicated PAN prep was serially diluted to 1/10 the stock concentration and supplied to both LPS +/- wells. 100 µL of the vehicle was supplied to the remaining wells. The plate was then incubated at 37ºC and 5% CO_2 for 16 hours. **(b)** 2,000,000 BMDMs were seeded in 1 mL of complete DMEM in a flat-bottom, 24-well plate with some wells primed for 1 hour according to the LPS co-incubation protocol. A 100-fold dilution was prepared of the stock PAN polymer and supplied to select wells. Cells were incubated at 37ºC and 5% CO_2. **(c)** Culturing parameters followed Figure 4.4b, with cells treated with unsonicated and extended sonication PAN preps. **(d)** Select PAN preps were prepared per Section 4.5.5 and incubated with cells primed with LPS at 150 ng/mL for one hour. Cells were dosed with nanoplastics and incubated at 37ºC and 5% CO_2. Significance was determined via a one-way ANOVA with a post hoc Tukey's test or a Welch's ANOVA with Brown-Forsythe, as discussed in Chapter 3, section 3.4.7. *$p < 0.05$, **$p < 0.01$, ***$p < 0.001$, ****$p < 0.0001$.

Figure 4.5. Differential gene expression (DGE) and gene set enrichment analysis (GSEA) for PAN microplastic-treated, co-incubation conditions, and controls for BMDMs. (a) Volcano plot illustrating differentially expressed genes enriched in LPS (red) or water (blue) conditions, with thresholds set at a log fold change of 1 and -1og10 adjusted p-value of 1.1. **(b)** Dotplot ranking normalized enrichment score (NES) against adjusted p-value in LPS (red) versus water (blue). **(c)** Volcano plot illustrating differentially expressed genes enriched in PAN microplastic plus LPS (red) or LPS control (blue) conditions, with thresholds used in Figure 4.5a. **(d)** Dotplot ranking normalized enrichment score (NES) against adjusted p-value in microplastic (red) versus vehicle control (blue). **(e)** Volcano plot illustrating differentially expressed genes enriched in MP plus LPS (red) versus LPS (blue) conditions, with thresholds described in Figure 4.5a **(f)** Dotplot ranking normalized enrichment score (NES) against adjusted p-value in MP (red) versus water (blue). **(g)** Heatmap representation of key genetic identifiers of macrophage M1 and M2 phenotypes.

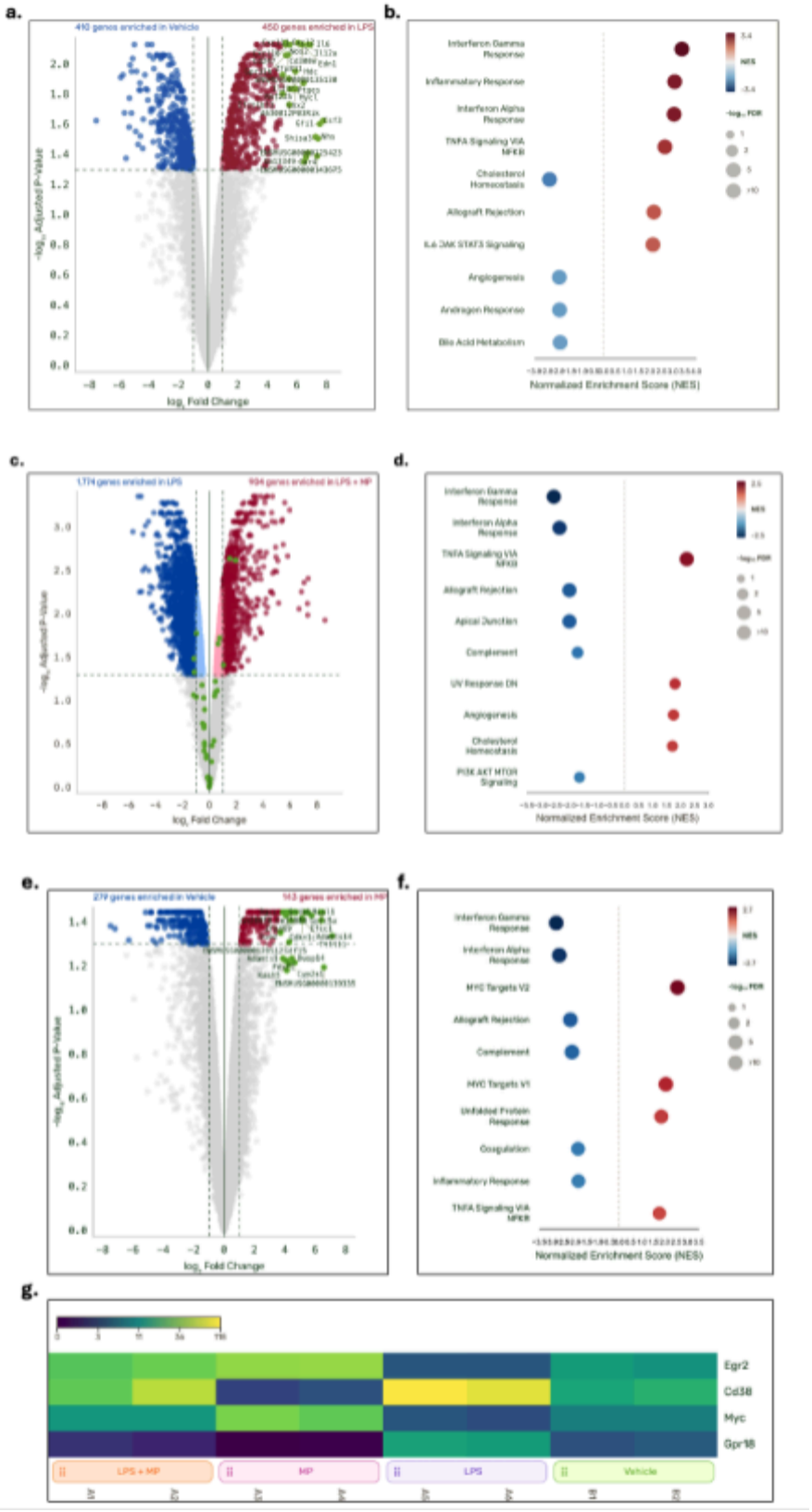
a.
410 genes enriched in Vehicle
450 genes enriched in LPS
log2 Fold Change
b.
Interferon Gamma Response
Inflammatory Response
Interferon Alpha Response
TNFA Signaling VIA NFKB
Cholesterol Homeostasis
Allograft Rejection
IL6 JAK STAT3 Signaling
Angiogenesis
Androgen Response
Bile Acid Metabolism
Normalized Enrichment Score (NES)
c.
1,714 genes enriched in LPS
934 genes enriched in LPS + MP
log2 Fold Change
d.
Interferon Gamma Response
Interferon Alpha Response
TNFA Signaling VIA NFKB
Allograft Rejection
Apical Junction
Complement
UV Response DN
Angiogenesis
Cholesterol Homeostasis
PI3K AKT MTOR Signaling
Normalized Enrichment Score (NES)
e.
279 genes enriched in Vehicle
163 genes enriched in MP
log2 Fold Change
f.
Interferon Gamma Response
Interferon Alpha Response
MYC Targets V2
Allograft Rejection
Complement
MYC Targets V1
Unfolded Protein Response
Coagulation
Inflammatory Response
TNFA Signaling VIA NFKB
Normalized Enrichment Score (NES)
g.
Egr2
Cd38
Myc
Gpr18
LPS + MP
MP
LPS
Vehicle

4.6 Tables

Table 4.1. Polymer preps used in treatment of bone marrow-derived macrophages. Preps listed below, including those in Tables 4.2 and 4.3, were incubated with BMDMs according to experimental need, and TNF-α secretion was quantified via ELISA.

Prep ID	Polymer	Fragmentation Modality	Time (min)	Concentration (mg/mL)	Z-average diameter (nm)	Diameter of Largest Peak (nm)
B1 Remake	PAN	Mechanical Fragmentation Sonication	30	34.30	737.47	841.27
PB1	PAN	Sonication	30	24.28	536.10	580.13
SB1	SAN	Sonication	30	20.05	508.33	499.97
BM1	PAN	Sonication	30	34.70	1575.0	1135.0
2H2	PAN	Sonication	90	32.00	1079.87	973.07
SAR2	PAN	Unsonicated	N/A	29.30	1826.0	1052.6

Table 4.2. PAN microplastic prep used for stimulation and bulk RNA sequencing. PAN stock polymer was prepared under the conditions listed above and then incubated with BMDMs.

Prep ID	Polymer	Fragmentation Modality	Time (min)	Concentration (mg/mL)	Z-average diameter (nm)	Diameter of Largest Peak (nm)
2H3	PAN	Sonication	90	25.50	1079.87	973.07

Table 4.3. PAN preps chosen for sterile filtration. Preps listed below were combined and filtered with a 0.22 μm filter and incubated with BMDMs according to Section 4.4.5.

Prep ID	Polymer	Fragmentation Modality	Time (min)	Concentration (mg/mL)	Z-average diameter (nm)	Diameter of Largest Peak (nm)
2H3	PAN	Sonication	90	25.50	1079.87	973.07
C4	PAN	Sonication	60	18.52	368.67	392.9

CHAPTER 5: EXPLORING HUMAN TRANSLATABILITY WITH PATIENT-DERIVED MONOCYTES

5.1 Introduction

Micro- and nanoplastics represent a multidimensional concern with environmental and physiological impact. Understanding of impact at the cellular level is limited, with studies exploring key targets such as cell signaling, cytotoxicity, and metabolism. Interactions driving these effects occur as various cell types are introduced to microplastics according to size, shape, and localization patterns. Plastics in the bloodstream indicate a particular problem, as size is a primary determinant of diffusive capacity across the intestinal or pulmonary epithelia and eventual interaction with leukocytes. Stock et al. analyzed the degree of transport in PE, PET, and PVC microplastics across a simulated intestinal epithelium with Caco-2 cells. With solely PE microplastics, they noted a small number of those sized 1 to 4 μm passed through the membrane, while cellular absorption occurred only for those < 5 μm. Sizes in the nanoscale range are interesting as they may act through paracellular absorption [22]. Regardless, this work suggests transport is size- and polymer-dependent, making discrete and potentially stimulating

interactions of specific particles in a polydisperse population with sentinel cells, such as circulating monocytes, more likely.

To study the impact of the soluble and insoluble interface (fractions) of PAN preps on human inflammatory responses, we obtained donor blood from the San Diego Blood Bank. Previously, Leonard et al., in performing chemical species and size characterization analysis in human whole blood samples, observed a diverse range of particle diameters and inflammatory responses. They cited an induced inflammatory response in PBMCs via IL-6 and TNF-α to polystyrene particles < 10 μm in size, and at higher concentrations, along with a reduction in cell viability [5].

PBMCs were isolated from immunocompetent patient-derived buffy coats after dilution and density-dependent centrifugation. Monocytes were selected for by plastic adhesion. TNF-α concentrations were measured post-incubation with a TNF-α ELISA and compared with BMDM and RAW 264.7 response profiles.

5.2 Results

5.2.1 Measurement of cytokine expression in patient-derived, adhesion-enriched monocytes

Three independent experiments, utilizing the previously described singular and co-incubation protocols in sections 3.4.3 and 3.4.4, detailed measurable differences in cytokine expression between experimental and control groups. The pilot experiment after density-dependent centrifugation, when treated with the original PAN vendor sonicated for 30 minutes at an incubation concentration of 0.1942 mg/mL, displayed significance in the solo microplastic condition versus the water control (Fig. 5.5a). When incorporating the new vendor with 30 minutes of sonication at 1.696 mg/mL, twice-tenfold serially diluted, and an unsonicated condition at 0.2344 mg/mL, the highest concentration in the sonicated prep incubation yielded

significant TNF-α output. Considering strictly unsonicated preps, with respective doses of Sarchem PAN at 2.244 and 0.2344 mg/mL and SPP at 2.263 and 0.2263 mg/mL, relative increases in cytokine output were observed despite lacking statistical significance.

5.3 Discussion

Monocyte-enriched PBMCs responded similarly to BMDMs and RAW 264.7 cells, with elevations of TNF-α observed in microplastic-only conditions at diluted concentrations and in conditions primed with 15 ng/mL LPS (Fig. 5.5a and 5.5b). Interestingly, it is plausible that the monocyte purity of the culture was the lowest of the three models, due to the reliance on adhesion enrichment. A heterogeneous culture, supporting other mononuclear cells such as lymphocytes and fully mature macrophages, provides a more representative and physiological network of cell interactions. A study by Wolff et al. details the density-dependent centrifugation of PBMCs and treatment with PMMA and PS. They noted a significant, concentration-dependent decrease in the inflammasome and an increase in genes associated with an M2 phenotype [27]. These results bolster those observed in our BMDMs and beckon a thorough evaluation of the physiological impacts of this bimodal response. Interestingly, the incubation of PBMCs with unsonicated SPP (1125.7 nm) and Sarchem PAN (1443.3 nm) generated large responses in TNF-α (although statistically insignificant) at the highest concentrations when primed with LPS, as compared to the plastic supplied independently. Despite the lack of response in previous cell types to Sarchem PAN, PBMCs exhibited an inflammatory response. Finally, with a lacking matched transcriptional sequencing dataset, it is compelling to consider whether human PBMCs exhibit a similar disordered M2 phenotype with conditional TNF-α preservation, as well as if a network of cell types aids or limits its onset.

5.4 Methods

5.4.1 Acquisition of patient-derived buffy coats and density-dependent centrifugation

A buffy coat was sourced from the San Diego Blood Bank from an anonymous donor. The coat was aliquoted and diluted fourfold with sterile PBS. Then, 14 mL of Lymphocyte Separation Medium (Corning; Corning, NY) was slowly dispensed to the bottom of the conicals until a clear interface was formed with the coat. Coats were spun at 1000g for 20 minutes at room temperature. After visual confirmation of the PBMC fraction, tubes were returned to the sterile hood. The upper cellular fraction was removed with plasma and pooled into a fresh 50 mL conical tube. Cells were spun at 500g for 5 minutes and decanted. 6 mL of ACK Lysing Buffer was supplied to dissociate residual red blood cells and incubated for 7 minutes at room temperature. An equivalent volume of sterile PBS was supplied post-incubation, and cells were spun at 500g for 5 minutes and decanted. Cells were resuspended in chilled complete RMPI medium (as in section 3.4.1) supplemented with 50% FBS and counted for cryopreservation.

5.4.2 Isolation and micro- and nanoplastic stimulation of adhesion-enriched monocytes

PBMCs were plated at 2,000,000 or 300,000 cells per well in a 24- or 96-well plate with 1 mL or 250 µL, respectively. Cells were incubated at 37ºC and 5% CO_2 for 24 to 48 hours to promote monocyte adhesion. The used media was discarded after incubation, and remaining PBMCs were supplied with complete RPMI + 10% FBS or RPMI + 10% FBS supplemented with 15 ng/mL LPS, as applicable. Cells were incubated at 37ºC and 5% CO_2 for 15 minutes. Then, the working concentration for the selected microplastic prep was serially diluted to 1/100 of the stock and supplied to both LPS-positive and negative wells at 8 to 10% of the culture

volume. Deionized water was supplied to the remaining wells. Plates were then incubated at 37 °C for 10 to 32 hours, as needed.

5.4.3 Enzyme-linked immunosorbent assay (ELISA) of supernatants

The BioLegend TNF-α ELISA MAX Deluxe kit was used following the manufacturer's protocols described in Chapter 3, section 3.4.5 for all microplastic stimulation experiments.

5.4.4 *Statistical analysis*

Statistical analysis for the ELISAs was performed using GraphPad Prism version 11.0.2 per Chapter 3, section 3.4.7.

5.5 Figures

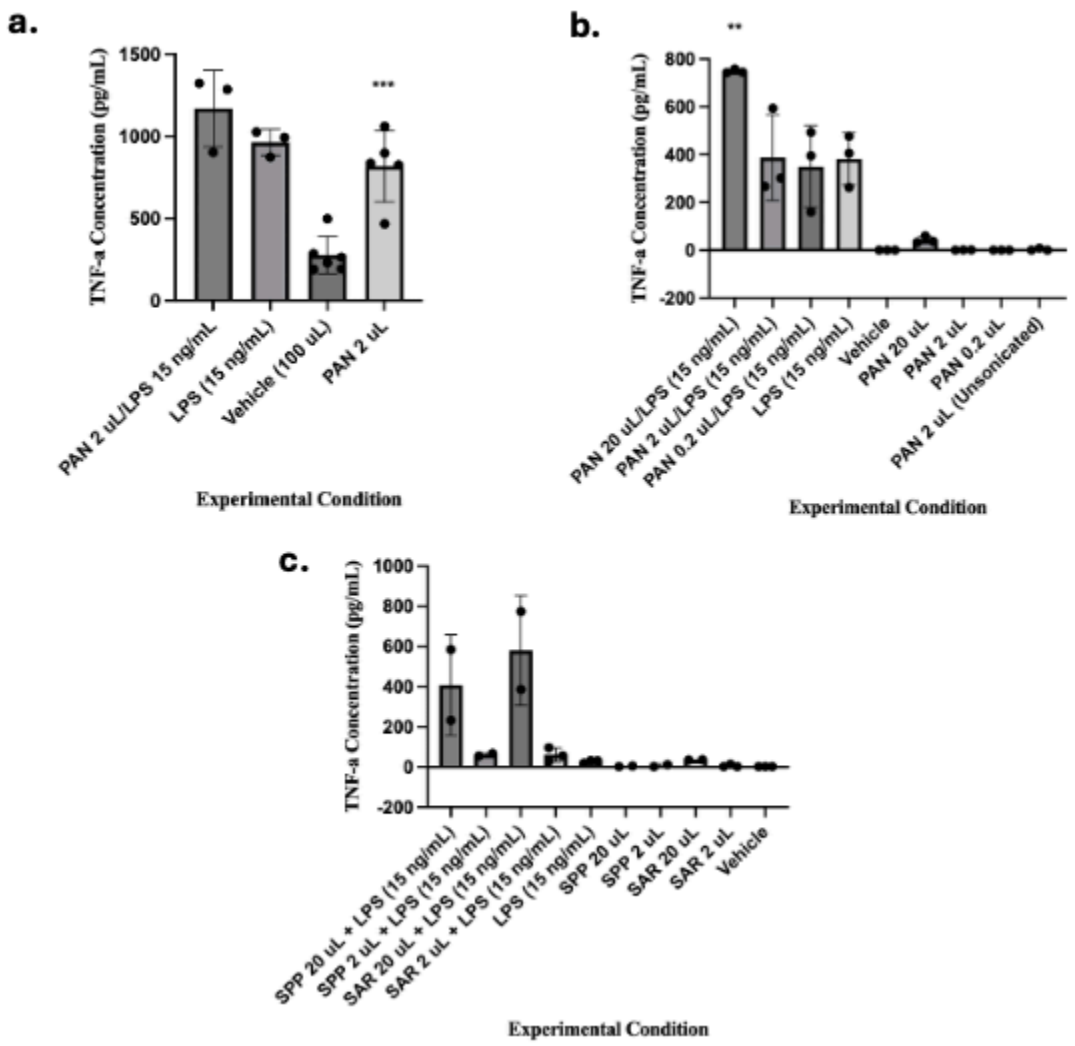

Figure 5.1. Evaluation of TNF-α in adhesion-enriched human monocytes using ELISA. (a) 2,000,000 cells were seeded across a 24-well plate in 1 mL of complete RMPI medium and allowed to adhere for 2 days. After 48 hours, the media were removed, and the remaining PBMCs were supplied with either RMPI and a vehicle control or RPMI containing 15 ng/mL LPS. A tenfold dilution of a PAN prep was prepared and supplied to cells. Cells were incubated for 24 hours at 37ºC and 5% CO_2. **(b)** A new PAN vendor was sourced, and 75,000 cells were cultured in a 96-well plate in 250 µL of complete RMPI for 18 hours. Afterward, cells were primed with LPS at 15 ng/mL for 15 minutes and then incubated with a 10x dilution of PAN for 10 hours. **(c)** 75,000 cells per well were cultured in a 96-well plate and incubated at 37ºC and 5% CO_2 for 24 hours. Cells were primed with conditions discussed in Figure 5.1b. PAN was tenfold diluted and supplied to both LPS +/- wells at stock and dilute concentrations. The cells were incubated at 37ºC for 32 hours. Significance was determined via a one-way ANOVA with a post hoc Tukey's test or a Welch's ANOVA with Brown-Forsythe, as discussed in Chapter 3, section 3.4.7. *$p < 0.05$, **$p < 0.01$, ***$p < 0.001$, ****$p < 0.0001$.

5.6 Tables

Table 5.1. Microplastic preps used to stimulate monocyte-enriched PBMCs. The preps listed below were incubated with monocyte-enriched PBMCs according to Section 5.4.2.

Prep ID	Polymer	Fragmentation Modality	Time (min)	Concentration (mg/mL)	Z-average diameter (nm)	Diameter of Largest Peak (nm)
PB1	PAN	Sonication	30	24.28	536.10	580.13
SAR2	PAN	Unsonicated	N/A	29.30	1826.0	1052.6
SAR1	PAN	Sonication	30	21.20	1443.3	931.2
NSPP	PAN	Unsonicated	N/A	28.20	2171.7	1125.7

CHAPTER 6: CONCLUSION

The burden of nano- and microplastics continues to threaten the biosphere. Persistent demand, production, and consumption aid in the introduction of plastics into the environment. Humans remain a target for microplastic accumulation, as respiratory and gastrointestinal routes provide a convenient point of ingress for particles of various shapes, sizes, and chemistries to invade the bloodstream and lodge in tissues, such as the liver or testicles. Notably, the water-soluble portion of plastics (like monomers) might be most suitable for biologic effects. Water-soluble plastic fragments can interact with the innate immune system, a dynamic and broadly positioned system responsible for establishing either pro- or anti-inflammatory cues. Considering this, we obtained the interface between the water-soluble and insoluble fraction of 14 unique plastic polymers. 6 of these 14 polymers contained microplastic fragments (1 to 5000 nm) as witnessed by DLS measurements. Of these, 9 were tested for ability to induce TNF-α in

RAW 264.7 cells *in vitro*. Only polyacrylonitrile (PAN) preps positively induced TNF-α production by RAW 264.7 cells.

Polyacrylonitrile, a compound with use cases in synthetic fibers, filtration membranes, biocompatible implants, and carbon fiber, illustrated consistent enrichment of TNF-α, a central pro-inflammatory cytokine, across multiple experiments in three distinct cell types. RAW 264.7 cells established the foundation for assessing general responsiveness, but their cell line identity weakens the interpretation of transcriptional signaling as physiologically relevant, especially in oncologically linked pathways like angiogenesis. Additionally, the most reproducible responses in RAW 264.7 cells required co-exposure to low-dose LPS.

Bone marrow cells produced a more robust and statistically consistent response to PAN, but saw reduction in TNF-α secretion when treated with a new PAN vendor or with a nanoplastic population < 0.22 μm. Unfortunately, the prep filtered for nanoplastics suffered from low concentration, relative to other preps supplied around 0.1 - 2 mg/mL. We must update the filtration protocols to obtain a truly representative population. Transcriptionally, the BMDM's highly significant upregulation of TNF-α matched its ELISA data, but related M1 cytokines were downregulated. A hybrid M1/M2 state is plausible; however, the potential for time-dependent programming is interesting in that cells may initially deploy resources for a traditional inflammatory response and shift to a recovery state.

Human PBMCs also responded to PAN fragments, even showing limited response to Sarchem PAN, which did not induce a response in the murine cells. Size is a clear distinguishing attribute between the two vendors, despite certain preps of SPP PAN inducing TNF-α at average diameters north of 500 nm. A logical thrust is to investigate the presence of a soluble or adsorbed contaminant. Knowing a confirmed chemical identity, FTIR data suggests a potential difference

in surface chemistry. Vectored materials, like bacteria, heavy metals, artifacts of the manufacturing process, or plasticizers, remain genuine concerns with proven physiological impact. More importantly, these data require a mechanistic evaluation to assess modes of binding to TLRs, phagocytosis, or production of ROS and generalized cytotoxicity. Additional future directions include addressing the lack of statistical power from limited sample sizes to obtain consistently significant differences among experimental groups while also aligning treatment concentrations to those experienced by cells *in vivo*. Finally, validation of sequencing data with quantitative mass spectroscopy and qPCR is needed.

Our study provides a unique, multisystem analysis of a sparsely studied compound in biological research. As synthetic polymer pollution persists in the natural environment, it has become increasingly important to study the interface of particles and the immune system. Plastics are a multidimensional problem with argued capacities to impact mammalian physiology as a function of size, shape, concentration, and polymer type, while facilitating introduction of known toxins and sequestration of proteins. Characterization efforts are essential to both classify and mitigate unnecessary exposure.

WORKS CITED

[1] B. P. Federation, “How Is Plastic Made? A Simple Step-By-Step Explanation,” British Plastics Federation. Accessed: Jun. 24, 2025. [Online]. Available: https://www.bpf.co.uk/plastipedia/how-is-plastic-made.aspx.

[2] I. E. Napper and R. C. Thompson, “Plastics and the Environment”.

[3] “Twenty years of microplastic pollution research—what have we learned?” Accessed: Jun. 13, 2025. [Online]. Available: https://www.science.org/doi/10.1126/science.adl2746.

[4] S. Goswami, S. Adhikary, S. Bhattacharya, R. Agarwal, A. Ganguly, S. Nanda, and P. Rajak, “The alarming link between environmental microplastics and health hazards with special emphasis on cancer,” *Life Sci.*, vol. 355, p. 122937, Oct. 2024, doi: 10.1016/j.lfs.2024.122937.

[5] S. V. L. Leonard, C. R. Liddle, C. A. Atherall, E. Chapman, M. Watkins, S. D. J. Calaminus, and J. M. Rotchell, “Microplastics in human blood: Polymer types, concentrations and characterisation using μFTIR,” *Environ. Int.*, vol. 188, p. 108751, Jun. 2024, doi: 10.1016/j.envint.2024.108751.

[6] L. C. Jenner, J. M. Rotchell, R. T. Bennett, M. Cowen, V. Tentzeris, and L. R. Sadofsky, “Detection of microplastics in human lung tissue using μFTIR spectroscopy,” *Sci. Total Environ.*, vol. 831, p. 154907, Jul. 2022, doi: 10.1016/j.scitotenv.2022.154907.

[7] S. Lee, K.-K. Kang, S.-E. Sung, J.-H. Choi, M. Sung, K.-Y. Seong, S. Lee, S. Y. Yang, M.-S. Seo, and K. Kim, “Toxicity Study and Quantitative Evaluation of Polyethylene Microplastics in ICR Mice,” *Polymers*, vol. 14, no. 3, Art. no. 3, Jan. 2022, doi: 10.3390/polym14030402.

[8] J. Li, J. Li, L. Zhai, and K. Lu, “Co-exposure of polycarbonate microplastics aggravated the toxic effects of imidacloprid on the liver and gut microbiota in mice,” *Environ. Toxicol. Pharmacol.*, vol. 101, p. 104194, Aug. 2023, doi: 10.1016/j.etap.2023.104194.

[9] H. Jin, T. Ma, X. Sha, Z. Liu, Y. Zhou, X. Meng, Y. Chen, X. Han, and J. Ding, “Polystyrene microplastics induced male reproductive toxicity in mice,” *J. Hazard. Mater.*, vol. 401, p. 123430, Jan. 2021, doi: 10.1016/j.jhazmat.2020.123430.

[10] S. S. Moosavi, H. Acevedo Ospina, and A. Descoteaux, “Polystyrene Nanoplastics Increase Macrophage Bactericidal Activity Through a Mechanism Involving Reactive Oxygen Species and Itaconate,” *Nanomaterials*, vol. 16, no. 2, p. 105, Jan. 2026, doi: 10.3390/nano16020105.

[11] C. Vanetti, M. Broggiato, S. Pezzana, M. Clerici, and C. Fenizia, “Effects of microplastics on the immune system: How much should we worry?,” *Immunol. Lett.*, vol. 272, p. 106976, Apr. 2025, doi: 10.1016/j.imlet.2025.106976.

[12] W. Yang, N. Jannatun, Y. Zeng, T. Liu, G. Zhang, C. Chen, and Y. Li, “Impacts of microplastics on immunity,” *Front. Toxicol.*, vol. 4, Sep. 2022, doi: 10.3389/ftox.2022.956885.

[13] M. Mohamadi, “Plastic Types and Applications,” in *Plastic Waste Treatment and Management: Gasification Processes*, R. Hasanzadeh and P. Mojaver, Eds., Cham: Springer Nature Switzerland, 2023, pp. 1–19. doi: 10.1007/978-3-031-31160-4_1.

[14] V. Tolardo, A. Romaldini, F. Fumagalli, A. Armirotti, M. Veronesi, D. Magrì, S. Sabella, A. Athanassiou, and D. Fragouli, “Polycarbonate nanoplastics and the in vitro assessment of their toxicological impact on liver functionality,” *Environ. Sci. Nano*, vol. 10, no. 5, pp. 1413–1427, May 2023, doi: 10.1039/D2EN00963C.

[15] J. Qin, B. Liang, Z. Peng, and C. Lin, “Generation of microplastic particles during degradation of polycarbonate films in various aqueous media and their characterization,” *J. Hazard. Mater.*, vol. 415, p. 125640, Aug. 2021, doi: 10.1016/j.jhazmat.2021.125640.

[16] H. Deng, U. Maitra, M. Morris, and L. Li, “Molecular Mechanism Responsible for the Priming of Macrophage Activation*,” *J. Biol. Chem.*, vol. 288, no. 6, pp. 3897–3906, Feb. 2013, doi: 10.1074/jbc.M112.424390.

[17] J. Parkin and B. Cohen, “An overview of the immune system,” *The Lancet*, vol. 357, no. 9270, pp. 1777–1789, Jun. 2001, doi: 10.1016/S0140-6736(00)04904-7.

[18] D.-W. Lee, J. Jung, S. Park, Y. Lee, J. Kim, C. Han, H.-C. Kim, J. H. Lee, and Y.-C. Hong, “Microplastic particles in human blood and their association with coagulation markers,” *Sci. Rep.*, vol. 14, no. 1, p. 30419, Dec. 2024, doi: 10.1038/s41598-024-81931-9.

[19] M. G. Bianchi, L. Casati, G. Sauro, G. Taurino, E. Griffini, C. Milani, M. Ventura, O. Bussolati, and M. Chiu, “Biological Effects of Micro-/Nano-Plastics in Macrophages,” *Nanomaterials*, vol. 15, no. 5, p. 394, Mar. 2025, doi: 10.3390/nano15050394.

[20] S. Liu, H. Li, J. Wang, B. Wu, and X. Guo, “Polystyrene microplastics aggravate inflammatory damage in mice with intestinal immune imbalance,” *Sci. Total Environ.*, vol. 833, p. 155198, Aug. 2022, doi: 10.1016/j.scitotenv.2022.155198.

[21] W. Zhou, X. Chen, J. Li, and J. He, “Long-term polystyrene nanoplastics exposure aggravates retinal inflammation and photoreceptor degeneration through microglial SPP1 signaling and neutrophil extracellular traps formation,” *J. Transl. Med.*, vol. 24, no. 1, p. 799, Jun. 2026, doi: 10.1186/s12967-026-08405-6.

[22] V. Stock, C. Laurisch, J. Franke, M. H. Dönmez, L. Voss, L. Böhmert, A. Braeuning, and H. Sieg, “Uptake and cellular effects of PE, PP, PET and PVC microplastic particles,” *Toxicol. In Vitro*, vol. 70, p. 105021, Feb. 2021, doi: 10.1016/j.tiv.2020.105021.

[23] M. Y. Adler, I. Issoual, M. Rückert, L. Deloch, C. Meier, T. Tschernig, C. Alexiou, F. Pfister, A. F. Ramsperger, C. Laforsch, U. S. Gaipl, K. Jüngert, and F. Paulsen, “Effect of micro- and nanoplastic particles on human macrophages,” *J. Hazard. Mater.*, vol. 471, p. 134253, Jun. 2024, doi: 10.1016/j.jhazmat.2024.134253.

[24] A. Schulze, M. Oshi, I. Endo, and K. Takabe, “MYC Targets Scores Are Associated with Cancer Aggressiveness and Poor Survival in ER-Positive Primary and Metastatic Breast Cancer,” *Int. J. Mol. Sci.*, vol. 21, no. 21, p. 8127, Oct. 2020, doi: 10.3390/ijms21218127.

[25] K. A. Jablonski, S. A. Amici, L. M. Webb, J. de D. Ruiz-Rosado, P. G. Popovich, S. Partida-Sanchez, and M. Guerau-de-Arellano, “Novel Markers to Delineate Murine M1 and M2 Macrophages,” *PLOS ONE*, vol. 10, no. 12, p. e0145342, Dec. 2015, doi: 10.1371/journal.pone.0145342.

[26] “Plasmidsaurus | Sequencing as a Service – RNA-seq Technical Documentation,” Plasmidsaurus. Accessed: Jul. 12, 2026. [Online]. Available: https://plasmidsaurus.com//technical-documentation/rna.

[27] C. M. Wolff, D. Singer, A. Schmidt, and S. Bekeschus, “Immune and inflammatory responses of human macrophages, dendritic cells, and T-cells in presence of micro- and nanoplastic of different types and sizes,” *J. Hazard. Mater.*, vol. 459, p. 132194, Oct. 2023, doi: 10.1016/j.jhazmat.2023.132194.